Endocytosis is a significant contributor to uranium(VI) uptake in tobacco (Nicotiana tabacum) BY-2 cells in phosphate-deficient culture

John, W.; Lückel, B.; Matschiavelli, N.; Hübner, R.; Matschi, S.; Hoehenwarter, W.; Sachs, S.;

Originally published:

February 2022

Science of the Total Environment 823(2022), 153700

DOI: https://doi.org/10.1016/j.scitotenv.2022.153700

Endocytosis is a significant contributor to uranium(VI) uptake in tobacco (*Nicotiana tabacum*) BY-2 cells in phosphate-deficient culture

Warren A. JOHN[a], Benita LÜCKEL[a], Nicole MATSCHIAVELLI[a], René HÜBNER[b], Susanne MATSCHI[c], Wolfgang HOEHENWARTER[c] and Susanne SACHS[a]*

[a]*Helmholtz – Zentrum Dresden-Rossendorf, Institute of Resource Ecology, Bautzner Landstraße 400, 01328 Dresden, Germany*

[b]*Helmholtz – Zentrum Dresden-Rossendorf, Institute of Ion Beam Physics and Materials Research, Bautzner Landstraße 400, 01328 Dresden, Germany*

[c]*Leibniz Institute of Plant Biochemistry, Weinberg 3, 06120 Halle (Saale), Germany*

* Correspondence to:

Dr. Susanne Sachs
Institute of Resource Ecology
Helmholtz – Zentrum Dresden-Rossendorf
Bautzner Landstraße 400,
01328 Dresden, Germany
Phone: +49 351 260 2436
E-mail: s.sachs@hzdr.de

Abstract

Endocytosis of metals in plants is a growing field of study involving metal uptake from the rhizosphere. Uranium, which is naturally and artificially released into the rhizosphere, is known to be taken up by certain species of plant, such as *Nicotiana tabacum*, and we hypothesize that endocytosis contributes to the uptake of uranium in tobacco. The endocytic uptake of uranium was investigated in tobacco BY-2 cells using an optimized setup of culture in phosphate-deficient medium. A combination of methods in biochemistry, microscopy and spectroscopy, supplemented by proteomics, were used to study the interaction of uranium and the plant cell. We found that under environmentally relevant uranium concentrations, endocytosis remained active and contributed to 14% of the total uranium bioassociation. Proteomics analyses revealed that uranium induced a change in expression of the clathrin heavy chain variant, signifying a shift in the type of endocytosis taking place. However, the rate of endocytosis remained largely unaltered. Electron microscopy and energy-dispersive X-ray spectroscopy showed an adsorption of uranium to cell surfaces and deposition in vacuoles. Our results demonstrate that endocytosis constitutes a considerable proportion of uranium uptake in BY-2 cells, and that endocytosed uranium is likely targeted to the vacuole for sequestration, providing a physiologically safer route for the plant than uranium transported through the cytosol.

Keywords: plant cell; proteomics; radionuclide transport; heavy metal interaction; vesicle uptake

1. Introduction

Uranium is a prime component of radionuclide waste emanating from the energy sector (Neill et al., 2018). This necessitates research into how this radionuclide can be safely stored, as well as possible worst-case scenarios in repositories such as ground- and pore-water ingress, which may result finally in leaching of radionuclides into soil and groundwater, thereby bringing it into contact with the environment. Compounded to that, naturally occurring uranium, of which ^{238}U is the most abundant isotope (99.3%), has lately been growing in infamy due to soil contamination resulting from natural processes, but more so from phosphate fertilization in agriculture as well as from mining activity (Schnug and Lottermoser, 2013; Wetterlind et al., 2012). Consequently, uranium in polluted ecosystems can enter the food chain through its uptake and translocation in certain plant species, and the ensuing bioaccumulation in entities at the top of the food chain can reach harmful and potentially lethal levels (Raskin et al., 1994). Since human beings are at the highest levels of the food chain, they are the most at risk. Although natural uranium has negligible radiotoxicity, it gives rise to potent chemical toxicity and poses serious threats to health (Craft et al., 2004). Nephrotoxicity has been observed to be the most prevalent outcome of uranium ingestion in humans and animals, for instance (Ribera et al., 1996).

Investigations into radioecological contamination and identifying potential long-term storage areas for radioactive waste are far from trivial, since such studies would have to account for many factors which affect the migration of radionuclides through soil. Uranium as an actinide element has a rather complex chemistry and therefore interaction with biological entities has to take into account the form in which it exists in solution, also referred to its chemical speciation because it impacts its bioavailability (Wall and Krumholz, 2006). The metal exists primarily in its hexavalent oxidation state in oxic soils and water bodies, i.e. U(VI), in the form of the uranyl(VI) ion UO_2^{2+} (Laroche et al., 2005; Wall & Krumholz, 2006). The uranyl(VI) ion has the propensity to form both soluble and insoluble complexes. Under acidic/near neutral conditions, the uranyl(VI) ion can form complexes with hydroxide and phosphate, and under alkaline conditions, with carbonate (Ebbs et al., 1998). Of the various complexes of U(VI), those with phosphate are the most stable and generally precipitate out of solution (Gorman-Lewis et al., 2009). Under reducing conditions, U(IV) is the predominant oxidation state and enters into stable complexes and often precipitates as uraninite (Langmuir, 1978).

Biological factors play a vital role in radionuclide migration through soil. Plants comprise a considerable proportion of the biomass of an ecosystem and are generally the entry points of uranium into the food chain. They require certain heavy metals such as Mn, Fe, Cu, Zn and Co in trace quantities for enzyme function and to act as cofactors for electron transport in photosynthesis (Andresen et al., 2018; Jeong and Connolly, 2009; Nicholas, 1975). Studies have revealed that the transport mechanisms used for these essential minerals are also employed by toxic metals and radionuclides such as uranium to enter the plant tissue (Song et al., 2017). Broad-spectrum ion channel transporters, such as the iron-regulated transporter 1 (IRT1) protein, regulate the influx of a range of metals (Nishida et al., 2011), making them vulnerable entry points for radionuclides. In the presence of uranium, metabolic pathways involved in iron uptake and homeostasis, for instance, have been observed to be affected (Doustaly et al., 2014). Moreover, there is evidence pointing towards calcium ion channels being responsible for uranium uptake (Rajabi et al., 2021; Sarthou et al., 2022).

Aside from transporter-mediated uptake, there has been mounting evidence of endocytosis-mediated uptake of metals. This has been observed in plants particularly for non-essential metals such as aluminium (Illéš et al., 2006; Wu et al., 2015), lanthanum (Ben et al., 2021; Wang et al., 2014), cadmium (Wang et al., 2014), lead (Hübner et al., 1985) and a host of other metals (Dragwidge and van Damme, 2020). Metal endocytosis is not only a reported feature in plant tissue but has also been observed in algae (Arunakumara and Zhang, 2007) and rodent kidneys (Zavala-Guevara et al., 2021). Just as in animal cells, endocytosis in plants is mainly a clathrin-mediated process and has so far been linked to the uptake and efflux of materials as well as the regulation of protein and lipid components of the plasma membrane (Murphy et al., 2005; Pérez-Gómez and Moore, 2007). The clathrin coat protein helps in initial invagination and subsequent budding of the lipid bilayer, resulting in the internalization of membrane-bound and extracellular constituents. Finally, dynamin-related GTPases complete the fission process to form a clathrin-coated vesicle (Fujimoto and Ueda, 2012). It is ultimately an energy-driven process, requiring guanosine-5’-triphosphate (GTP) for vesicle formation and subsequent trafficking, which is thought to be aided by a myriad of Rab-GTPases as demonstrated by Nielsen et al. (2008). The trafficking of an endocytic vesicle depends on the cargo it is carrying. A new vesicle fuses with early endosomes or the trans-Golgi network where it is then either transported back to the plasma membrane for recycling or targeted to the vacuole through late endosomes or multi-vesicular bodies for degradation or storage (Ekanayake et al., 2019; Wang et al., 2020). To investigate endocytosis in plant cells, styryl

dyes such as FM4-64™ have been well-established due to their ability to bind to plant cell membranes and be internalized, while not conferring major toxicity (Rigal et al., 2015).

Currently, there is a wealth of information concerning the uptake of uranium by various species of plants (Chen et al., 2021; Ebbs et al., 2000; Jessat et al., 2021; Ratnikov et al., 2020; Rodriguez-Freire et al., 2021; Saenen et al., 2013; Shahandeh and Hossner, 2002; Soudek et al., 2014; Stojanović et al., 2012; Viehweger and Geipel, 2010). The majority of these studies deal principally with uptake rates of the radionuclide for the purpose of phytoremediation, and a meagre, albeit growing, number attempt to shed light on mechanisms. So far, the most investigated mechanisms of uranium uptake pertain to ion-channels (Berthet et al., 2018; Doustaly et al., 2014; Gupta et al., 2020; Rajabi et al., 2021; Sarthou et al., 2022). In this light, the aforementioned evidence arguing for an endocytosis-mediated uptake of metals, led us to hypothesize that vesicular uptake is one mechanism of uranium transport into plant cells.

Notwithstanding, investigating interactions of plants with uranium is a challenging feat due to the use of inorganic phosphate in cultures, which would cause uranium to precipitate out of solution and render it unavailable to the plant (Ebbs et al., 1998). Phosphate is a crucial component of cellular growth and development, and is needed for plasma membrane integrity, energy, nucleic acid biosynthesis, signalling, *etc*. (Mimura, 1995). Deficiencies in phosphate availability would therefore have detrimental effects to cell growth and replication (Sano et al., 1999).

In this study, we devised an experimental setup to circumvent the adverse effects of phosphate deficiency in tobacco (*Nicotiana tabacum*) bright yellow 2 (BY-2; Nagata et al., 1992) cell suspensions in order to investigate the uptake of uranium via endocytosis into these cells. The model organism tobacco has been a reputable workhorse in heavy metal research (Rehman et al., 2019) and is also known to have pronounced accumulation rates of uranium (Rajabi et al., 2021; Soudek et al., 2014; Stojanović et al., 2012). The undifferentiated BY-2 cell line was selected due to its ease of handling and the easier visualization of cellular processes taking place. With the help of proteomics, combined with methods in classical molecular biology involving microscopy, we ascertained that endocytosis remains active in the presence of uranium and is involved in its uptake into the cell.

2. Materials and Methods

2.1. Cell culture

Tobacco BY-2 cells were grown as outlined in Rajabi et al. (2021) in modified Murashige-Skoog (MS) medium (4.3 g l^{-1} MS basal salt, 200 mg l^{-1} KH_2PO_4, 30 g l^{-1} sucrose, 100 mg l^{-1} myo-inositol, 1 mg l^{-1} thiamine hydrochloride and 0.2 mg l^{-1} 2,4-dichlorophenoxyacetic acid; 2,4-D, pH 5.8) in the dark at 25°C on an IKA®KS 260 basic orbital shaker (IKA Labortechnik, Staufen, Germany) set to 150 rpm. Consult appendix for details of chemicals and reagents. pH values were measured with a pH meter (inoLab pH Level 1, WTW, Weilheim, Germany) using a BlueLine 16 pH electrode (SI Analytics, Mainz, Germany). Sub-cultivation was performed on a weekly basis, with 1 ml of culture being added to 30 ml of MS medium in 100-ml sterile Erlenmeyer flasks.

2.2. Exposure of BY-2 cells to uranyl(VI) nitrate

Cells were first cultured in MS medium for 96 h according to the standard culture conditions as mentioned in the preceding section. An appropriate volume, based on the experiment, of this 96-h old culture was then added into 30 ml of phosphate-deficient MS (MS_{red}) medium (0.026 mg l^{-1} $CoCl_2 \cdot 6H_2O$, 0.025 mg l^{-1} $CuSO_4 \cdot 5H_2O$, 0.25 mg l^{-1} $Na_2MoO_4 \cdot 2H_2O$, 331.9 mg l^{-1} $CaCl_2$, 1900 mg l^{-1} KNO_3, 1650 mg l^{-1} NH_4NO_3, 6.2 mg l^{-1} H_3BO_3, 0.83 mg l^{-1} KI, 16.9 mg l^{-1} $MnSO_4 \cdot H_2O$, 8.6 mg l^{-1} $ZnSO_4 \cdot 7H_2O$, 180.54 mg l^{-1} $MgSO_4 \cdot 7H_2O$, 9.3 mg l^{-1} KCl, 36.7 mg l^{-1} FeNaEDTA, 1.7 mg l^{-1} KH_2PO_4, 30,000 mg l^{-1} sucrose, 100 mg l^{-1} myo-inositol, 1 mg l^{-1} thiamine hydrochloride and 0.2 mg l^{-1} 2,4D; pH adjusted to 5.8 with KOH) in 100-ml Erlenmeyer flasks. Cells were cultured in MS_{red} medium with reduced phosphate in order to limit the formation of uranyl(VI) phosphate precipitates. Sterile uranyl(VI) nitrate from stock solutions of approximately 10 mM was then added to predetermined concentrations, depending on the experiment, and left to incubate for a designated period under culture conditions. The experimental conditions and concentrations of uranium used were based on previous toxicological analyses of uranium in tobacco BY-2 by Rajabi et al. (2021) except without any preconditioning of BY-2 cells in MS_{red} medium. Uranium in natural isotope composition is a radioactive α emitter. It should be handled in dedicated facilities with appropriate equipment for radioactive materials to avoid health risks caused by radiation exposure.

2.3. Determining phosphate content in BY-2 culture in MS medium

In triplicate, cells were sub-cultivated into 30 ml of fresh MS medium and incubated under culture conditions. 1.5 ml of the culture were sampled from the flask after 0, 24, 48, 72 and 96 h of incubation and cells were separated by centrifuging at 16,000 *g* for 10 min with a 5804R table-top centrifuge (Eppendorf AG, Hamburg, Germany). 1 ml of each supernatant was acidified with 10 µl of distilled HNO_3 in order to solubilize and stabilize all ions. Phosphorus content was then determined by inductively coupled plasma mass spectrometry (ICP-MS). For ICP-MS measurements, a NexION 350x spectrometer (Perkin Elmer, Rodgau, Germany) with an operating radio frequency power (RFP) of 1300 W or an iCap RQ spectrometer (Thermo Fisher Scientific, Dreieich, Germany) with an RFP of 1550 W, were used. Both machines were equipped with quadrupole mass analysers. Elements were analysed using either helium mode with kinetic energy discrimination or standard mode. Three measurements were performed per sample using argon plasma gas and internal standards of rhodium, scandium and lutetium.

2.4. Cell growth and viability in phosphate-deficient culture

5 ml of a 96-h culture in MS medium were added to three Erlenmeyer flasks containing 30 ml of MS_{red} medium and one flask containing 30 ml of MS medium. All four flasks were left to incubate under culture conditions. Phase contrast images of cells were acquired with an Axiovert 40 CFL light microscope (Carl Zeiss Microscopy GmbH, Oberkochen, Germany).

Cell viability experiments were performed according to Rajabi et al. (2021). Cells were separated from culture using 37-µm pore size nylon membranes (Bückmann, Mönchengladbach, Germany) placed in CellCrown™ inserts (Sigma-Aldrich, Taufkirchen, Germany) to function as filters in 12-well plates (Greiner, Frickenhausen, Germany) and then stained with a 2.5% (w/v) solution of Evans Blue reagent in MilliQ water for 3 min. Destaining was done by rinsing the cells at least three times in MS_{red} medium. Using a Fuchs-Rosenthal counting chamber (Brand GmbH & CO KG, Wertheim, Germany), up to 500 cells were counted, with six individual counting events per sample, and the ratio of non-stained cells to the total number of cells was calculated in order to determine viability. The standard error of the mean (SEM; Eq. 1) was calculated for each testing condition and was represented according to Altman & Bland (2005) and a two-tailed student's t-test was used to evaluate statistical significance between measurements at 0 and 24 h.

$$standard\ error\ of\ the\ mean = \frac{sample\ standard\ deviation}{\sqrt{number\ of\ samples}} \qquad \text{Eq. (1)}$$

Cell growth was determined by measuring dry biomass. 1.5 ml of each culture were spun down using a 5415R table-top centrifuge (Eppendorf AG, Hamburg, Germany) for 10 min at 16,000 *g* in pre-weighed 1.5-ml centrifuge tubes. Cells were washed twice with MilliQ water and centrifugation was used to remove each wash. The cell masses were subsequently freeze-dried using an Alpha 2-4 LSCbasic lyophilizer (Martin Christ Gefriertrocknungsanlagen GmbH, Osterode am Harz, Germany) and the dry cell mass in each tube was determined by weighing the centrifuge tubes on an ultra-fine balance. SEM was calculated for each testing condition and significance between measurements at 0 and 24 h was calculated using a two-tailed student's t-test.

2.5. Visualization of endocytosis

2 ml of a 96-h culture in MS medium were added to three Erlenmeyer flasks, each containing 30 ml of MS_{red} medium. To one flask, wortmannin was added to a final concentration of 5 µM to inhibit endocytosis (Jelínková et al., 2015) and allowed to incubate for 40 min under culture conditions to serve as a positive control for endocytic blocking. To this flask and a flask without wortmannin, uranyl(VI) nitrate was added to a concentration of 20 µM. The third flask was maintained as a negative control with the absence of both U and wortmannin, and all flasks were allowed to incubate for 5 h under culture conditions.

Following incubation, all cultures were placed on ice for 15 min to temporarily inhibit endocytosis and FM4-64™ dye was added to a working concentration of 1.65 µM to stain lipid membranes. Live staining was done by shaking the cells at 25°C in the dark for 90 min. Fluorescence microscopy was subsequently performed on this suspension with an AxioObserver Z1 microscope using a 530-nm Colibri excitation source and an HE60 filter set (Carl Zeiss Microscopy GmbH, Oberkochen, Germany) to visualize the FM dye. General physiology was examined using transmitted light with phase contrast. Acquisition was performed with the AxioVision (v4.8) software using a fixed camera exposure time for the FM dye.

Quantification of intracellular FM4-64 signals was performed using ImageJ (National Institutes of Health) by measuring mean intensities of drawn regions of interest, which only constituted the inside of the cell and excluded any peripheral staining. Cells were counted from one biological replicate from each testing condition, with two to three locations being considered. The number of cells counted for the control was 61, for the U-treated sample, 43,

and for the U+WM-treated sample, 42. These mean intensities were normalized to the background mean intensities in each image. Statistical analysis was then done in the form of a two-tailed student's t-test to show significance.

2.6. Proteomics analysis

5 ml of a 96-h culture in MS medium were added to 30 ml MS_{red} medium in six flasks. To three of these flasks, uranyl(VI) nitrate was added to a concentration of 10 µM and the remaining three flasks served as negative controls (i.e. three biological replicates per testing condition). All six cell suspensions were incubated for 24 h under culture conditions.

For protein extraction, a modified method based on that by Laing & Christeller (2004) was used. 10 ml of each cell suspension were washed once with ice-cold 3-(N-morpholino)propanesulfonic acid (MOPS) buffer (50 mM, pH 7.5). The cells were resuspended in 1 ml of ice-cold lysis buffer (1% Triton™ X-100, 2 mM dithiothreitol, 5% polyvinylpolypyrrolidone, 50 mM MOPS, cOmplete™ protease inhibitor according to manufacturer's instructions, pH 7.5) and ground to a fine powder using liquid nitrogen. Protein extract was obtained by centrifuging at 16,000 *g* for 20 min at 4°C. A small aliquot of the extract was mixed with four parts of ice-cold acetone in order to precipitate and concentrate proteins. The protein concentration was determined using a Pierce™ Coomassie Plus (Bradford) Assay Kit (Thermo Scientific, Rockford, IL, USA) according to the manufacturer's instructions.

Proteins in solution were digested and desalted according to Majovsky et al. (2014). Consult appendix for details on protein digestion. Dried peptides were dissolved in 5% acetonitrile (ACN), 0.1% trifluoroacetic acid and were injected into an EASY-nLC 1000 liquid chromatography system (Thermo Fisher Scientific). Peptides were separated using liquid chromatography C18 reverse phase chemistry employing a 550 min gradient increasing from 5% to 40% ACN in 0.1% formic acid, and a flow rate of 250 nl min^{-1}. Eluted peptides were electrosprayed on line into a QExactive Plus mass spectrometer (Thermo Fisher Scientific). The spray voltage was 1.9 kV, the capillary temperature 275°C and the Z-Lens voltage 240 V. A full mass spectrometry (MS) survey scan was carried out with chromatographic peak width set to 15 s, resolution set to 70,000, automatic gain control (AGC) at $3x10^6$ and a max injection time (IT) of 100 ms. MS/MS peptide sequencing was performed using a Top10 data dependent acquisition (DDA) scan strategy with high collision dissociation (HCD) fragmentation. MS scans with mass to charge ratios (m/z) between 400 and 1850 were acquired. MS/MS scans

were acquired with a resolution of 17,500, AGC of $5x10^4$, IT of 50 ms, isolation width of 1.6 m/z, normalized collision energy of 28, under fill ratio of 3%, dynamic exclusion duration of 20 s, and an intensity threshold of $3x10^4$.

MS/MS spectra were used to search the *Nicotiana tabacum* database from UniProt with the Mascot software v.2.5 linked to Proteome Discoverer v.2.1 (Orsburn, 2021). The enzyme specificity was set to trypsin and lysyl endopeptidase, and two missed cleavages were tolerated. Carbamidomethylation of cysteine was set as a fixed modification and oxidation of methionine as a variable modification. The precursor tolerance was set to 7 ppm and the product ion mass tolerance was set to 0.8 Da. A decoy database search was performed to determine the peptide spectral match (PSM) and peptide identification false discovery rates (FDR). PSM, peptide and protein identifications surpassing respective FDR thresholds of $q < 0.01$ were accepted. MS raw data were imported into the Progenesis software v4.2 (Waters Corportation, Milford, MA, USA) which performs alignment of liquid chromatography-mass spectrometry (LC-MS) measurements, peptide ion signal peak picking in the aligned data, normalization and peak integration to quantify peptide ion signals across LC-MS measurements. Peptide ion signal abundance was used to quantify cognate proteins using the non-conflicting peptides protein quantification index (PQI). Only peptides that showed an in-group coefficient of variance of < 30% and cognate proteins with an ANOVA multiples testing corrected q-value < 0.05 were retained and considered differentially expressed. The mass spectrometry proteomics data have been deposited to the ProteomeXchange Consortium via the Proteomics Identification Database (PRIDE; Perez-Riverol et al., 2019) partner repository with the dataset identifier PXD028677 and 10.6019/PXD028677.

2.7. Endocytosis-mediated uranium bioassociation

4.5 ml of a 96-h culture in MS medium were added to three Erlenmeyer flasks, each containing 30 ml MS_{red} medium. To one of these cultures, wortmannin was added to a final concentration of 33 µM and this flask was cultured for 30 min. To the wortmannin-treated culture and a second flask of MS_{red} culture, uranyl(VI) nitrate was added to a concentration of 20 µM. The third flask served as a control. All flasks were incubated for 6 h under culture conditions. Cells were subsequently separated from the culture medium through vacuum filtration and rinsed on the filter with 30 ml of MilliQ water. In triplicate, 100 µg of the washed cell residue were weighed out into 15-ml centrifuge tubes and digested in 3 ml of a solution of 10% H_2O_2 and 43% HNO_3 by heating to 80°C for 4 h. Once cooled, the volume was topped up to 5 ml with MilliQ water and elemental analysis in both the culture medium and cell extracts

was carried out by ICP-MS. SEM was calculated for each testing condition and significance between the wortmannin-treated and -untreated samples was evaluated using a two-tailed student's t-test.

2.8. Preparation for transmission electron microscopy

BY-2 cells exposed to 0, 20 and 200-µM concentrations of uranyl(VI) nitrate in MS_{red} medium for 24 h were embedded in 2% agar. Preparations for transmission electron microscopy (TEM) were done using modified methods of those outlined in Mulisch & Welsch (2010) with ethanol substitution and Spurr's resin infiltration (Spurr, 1969). Consult appendix for details. The resin blocks were then trimmed and thin sections (< 100 nm) were obtained using an EM UC7 ultramicrotome (Leica Microsystems GmbH, Wetzlar, Germany). The thin sections were mounted on carbon-coated copper grids and contrasted using lead citrate as described by Reynolds (1963). The thin sections containing cells unexposed to uranium were additionally contrasted with 2.5% uranyl(VI) acetate.

2.9. Transmission electron microscopy and spectrum imaging analysis

For all TEM-based analyses, the section-containing grids were placed in a high-visibility low-background holder and decontaminated for 2 s in a Model 1020 Plasma Cleaner (Fischione, Export, PA, USA). A Titan 80-300 electron microscope (FEI, Eindhoven, Netherlands) operating at an accelerating voltage of 300 kV was used to acquire bright-field TEM micrographs. For selected positions on each section, high-angle annular dark-field scanning transmission electron microscopy (HAADF-STEM) and spectrum imaging analysis based on energy-dispersive X-ray spectroscopy (EDX) were performed with a Talos F200X microscope equipped with a high-brightness X-FEG electron source and a Super-X EDX detector system (FEI) at an accelerating voltage of 200 kV. Using the ESPRIT software version 1.9 (Bruker), two-dimensional element distributions were obtained after Bremsstrahlung background correction based on the physical TEM model and series fit peak deconvolution. For representation, selected element maps were overlaid using ImageJ and the Correlia plug-in (Rohde et al., 2020).

3. Results

3.1. Alleviating stress caused by phosphate deficiency

The standard method of BY-2 cell culture was in MS medium. However, in order to properly expose BY-2 cells to bioavailable uranium, it was necessary to keep the formation of insoluble uranium complexes in culture medium to a minimum. Hence, the cells were cultured in phosphate-deficient MS_{red} medium, containing only 1.7 mg l^{-1} phosphate (as opposed to 200 mg l^{-1} in MS medium), when they were exposed to uranyl(VI) nitrate. Moreover, it had to be ensured that the phosphate content of the MS medium culture had dropped below a threshold of 1.7 mg l^{-1} to avoid a carryover of phosphate during the transfer of the culture into MS_{red} medium. ICP-MS measurements revealed that phosphate content of the cell-free MS medium after 96 h of BY-2 culture was 238 ± 45 µg l^{-1} and thus well-below the threshold (see Appendix A Fig. **A.1**). A previous study showed that cells are still in a late-exponential phase of growth after 96 h of culture in MS medium (Srba et al., 2016), which was also confirmed through our own experiments by analysing cell growth over one week in MS medium (data not shown). Therefore, the following exposures of BY-2 cells to uranyl(VI) nitrate were performed with cultures grown for 96 h in MS medium transferred to fresh MS_{red} medium.

A lack of phosphate, however, is not conducive to the healthy growth of plant cells. Accordingly, further inquiry was warranted to ensure that uranium-exposed cells were not being additionally stressed as a result of a deficiency of phosphate in the culture. To confirm this, the effects of a 24-h incubation of cells in phosphate-deficient conditions were assessed by cell viability and cell growth (measured by dry biomass). After 24 h of growth in fresh MS_{red} culture compared to a fresh MS culture, the difference in cell viability was minor and cultures still consisted of populations with over 90% viable cells (Fig. **1a**). Furthermore, cell mass approximately doubled within 24 h of phosphate deficiency, showing that cells continued to replicate (Fig. **1b**). Sano et al. (1999) showed that the mitotic index decreases to 0% when BY-2 cells are kept in phosphate-deficient conditions for 72 h. Therefore, the progress of the cell cycle over a 24-h time frame in this instance argues for cells that were not yet experiencing high stress due to a lack of phosphate. This was additionally confirmed by light microscopy, revealing the physiology of cells in MS_{red} for 24 h to be similar to those in MS medium (Fig. **1c, d**) However, cells grown for upwards of 72 h in MS_{red} had greater populations of larger cells and showed a more adverse appearance, with what appeared to be aggregations of large vesicles, usually representative of cell death processes (Fig. **A.2**; Hiraga et al., 2010). It was

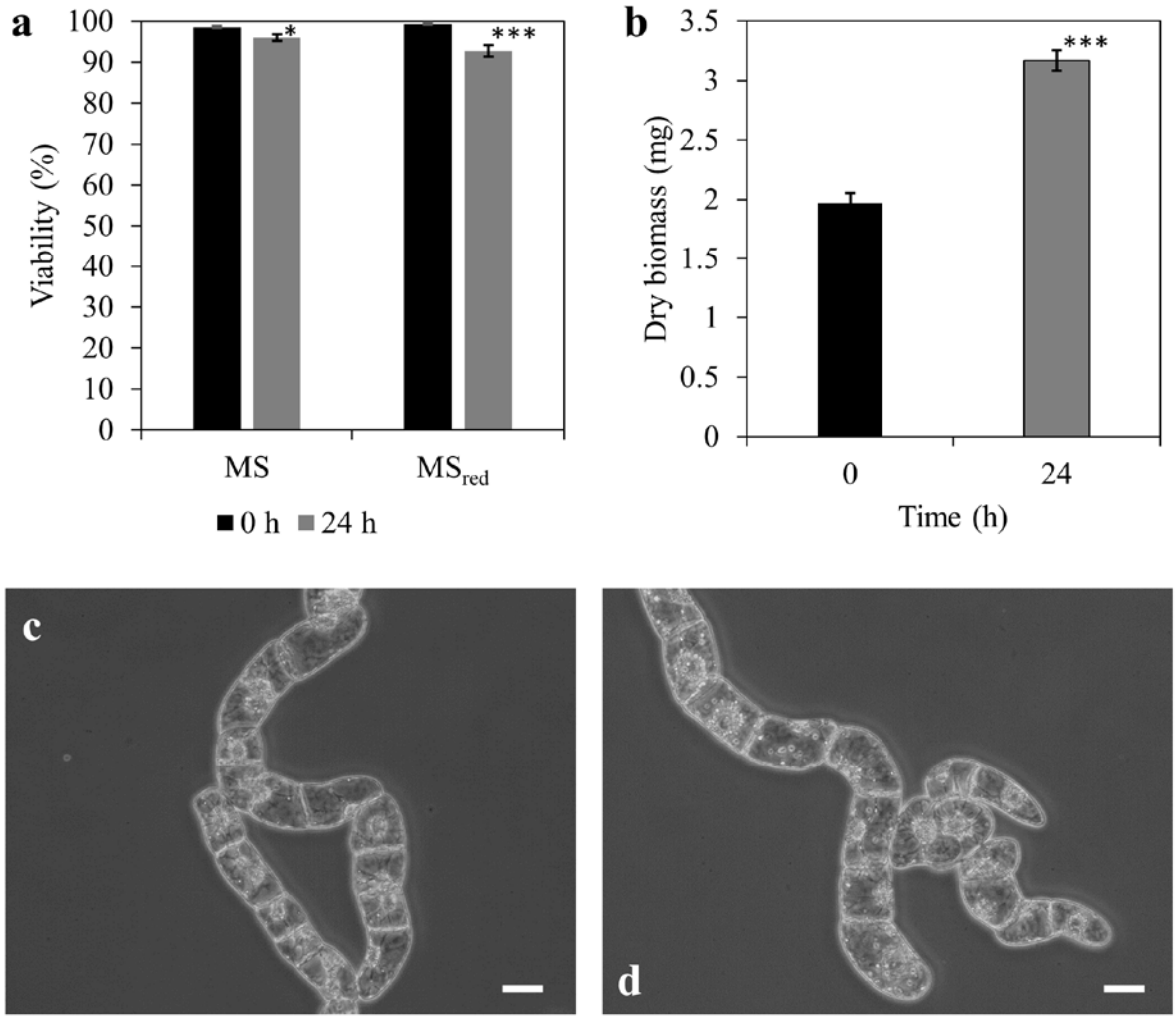

Fig **1**: Cell viability (a) and dry biomass (b) of a 96-h old tobacco BY-2 culture in MS medium sub-cultivated into MS_{red} and grown for 24 h. Error bars represent standard errors of the mean for one biological replicate with three counting events for MS medium and three biological replicates each with three counting events for MS_{red} medium. Statistical significance is denoted by * ($p < 0.05$) and *** ($p < 0.001$) between corresponding 0-h and 24-h samples. Micrographs of BY-2 cells before (c) and after (d) 24 h in MS_{red} medium. Scale bar: 20 µm.

thus determined that cells cultured for up to 24 h in phosphate-deficient conditions were sufficiently vital for further investigations with uranium exposure.

3.2. Endocytosis remains active in the presence of uranium

Endocytosis in the presence of uranium was firstly examined using fluorescence microscopy. The styryl dye FM4-64™ is a compound that intercalates within moieties of the plasma membrane, causing it to fluoresce, and is therefore a useful marker for vesicular uptake as it migrates over time into the cell during live staining (Bolte et al., 2004). Cells were exposed to 20 µM uranyl(VI) nitrate for 5 h and subsequently stained with FM4-64™. An exposure to 20 µM uranium was chosen because, firstly, it resembles uranium concentrations in soil that is

mildly contaminated (Vandenhove, 2002), and secondly, it induces a level of toxicity over 24 h without completely killing the cell population (Fig. **A.3**). The relatively short exposure meant that cells were within the limits of experiencing stress due to phosphate deficiency and also to the presence of uranium. The viability of these cells was still relatively high at 80 ± 3% with exposure to 20 µM uranium for 6 h and thus meant that there was minimal compromise to plasma membrane integrity caused by uranium.

It was evident that in both the presence and absence of uranium, the dye was taken up (Fig. **2a-d**). After 90 min of live staining, an intracellular staining pattern emerged, proving that endocytosis was still in play in both conditions. Consistent with these findings, Bolte et al. (2004) reported a staining of numerous organelle membranes in BY-2 cells within 1 h of dye incubation. The observation that both the uranium-treated and control experiments showed staining under 90 min would imply that the rate of vesicular uptake remained largely unhindered in the presence of uranium.

Wortmannin is a phosphoinositol-3-kinase (PI3K) inhibitor and has been widely used in applications to artificially block endocytosis in plant cells (Jelínková et al., 2015). To test the effects of actual endocytosis impairment on the staining pattern of FM4-64™, cells were treated with wortmannin for 30 min prior to staining. In this case, even after 90 min of incubation with FM4-64™, there was only peripheral staining (Fig. **2e, f**), indicating that the dye was unable to migrate into the cell via vesicular uptake. A quantification of the intracellular staining pattern, discounting any peripheral signals, showed that cells treated with wortmannin showed a strongly reduced mean intensity signal within the cells compared to the other testing conditions, which also showed strong statistical significance between the wortmannin-treated and -untreated samples. (Fig **3**). This demonstrates that unlike other metals, which have been seen to inhibit endocytosis (Fan et al., 2011; Wang et al., 2014), the presence of uranium at a concentration of 20 µM does not have an inhibitory effect on endocytosis.

To verify this observation, abundance levels of proteins responsible for vesicular uptake via clathrin-mediated endocytosis (CME) were analysed using a proteomics approach. Relative protein abundance was analysed in cells exposed to uranyl(VI) nitrate in fresh MS_{red} medium and compared to a control experiment in MS_{red} without uranium. To elicit a distinct protein response to the presence of uranium in culture, experiments were conducted using a longer uranium exposure time of 24 h and, thus, a lower

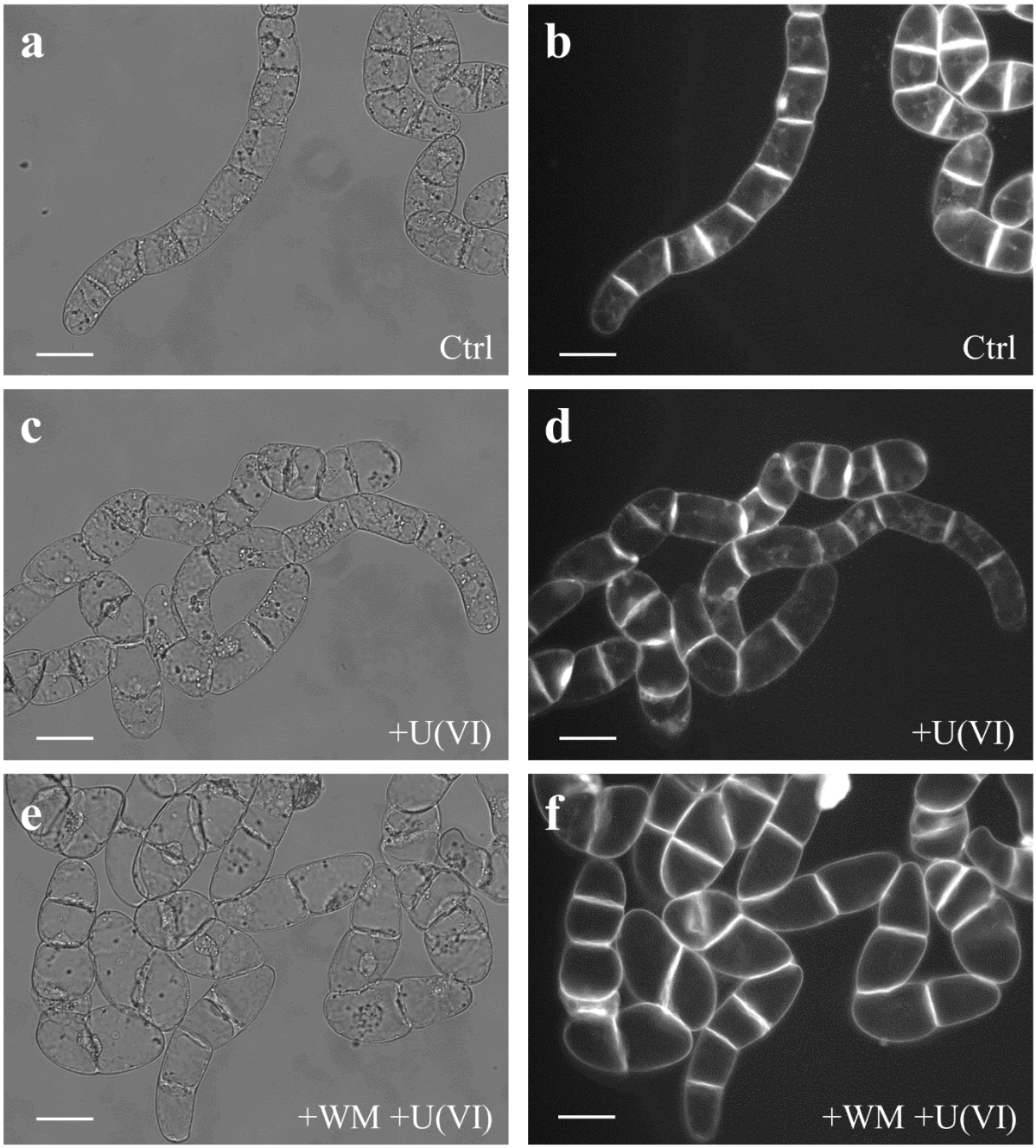

391

Fig **2**: Internalisation of the FM4-64™ stain after 90 min of dye exposure in untreated tobacco BY-2 cells (Ctrl), cells treated with 20 µM uranyl(VI) nitrate and cells treated with both 20 µM uranyl(VI) nitrate and 5 µM wortmannin (WM). Cell physiology is shown by phase contrast images (a, c and e), and endocytosis is shown by FM4-64™ fluorescence (b, d and f). Scale bar: 50 µm.

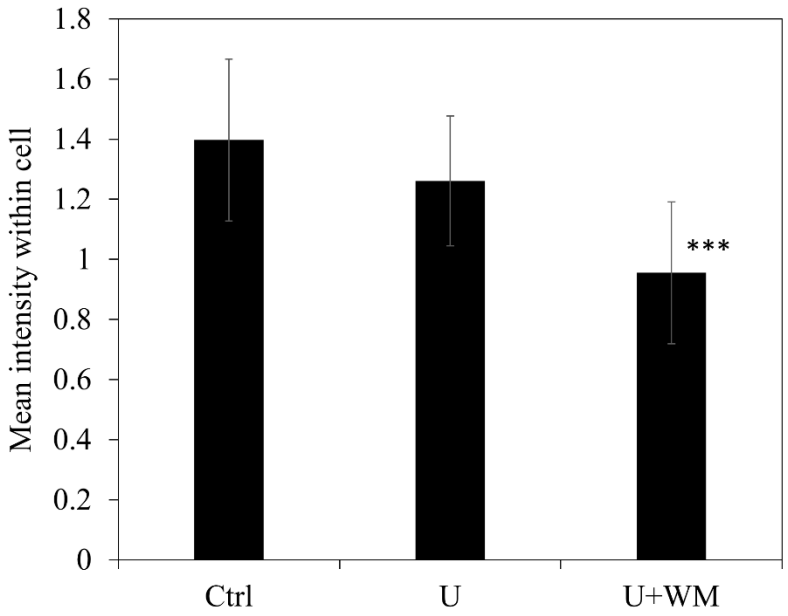

Fig **3**: Signal intensities within the cell after 90 min of FM4-64™ in untreated tobacco BY-2 cells (Ctrl; n=61), cells treated with 20 µM uranyl(VI) nitrate (U; n=43) and cells treated with both 20 µM uranyl(VI) nitrate and 5 µM wortmannin (U+WM; n=42). Measurements are taken from at least two sampling events from one biological replicate for each testing condition. Statistical significance is denoted by *** ($p < 0.001$) between U and U+WM and n represents the number of cells per field of view.

uranium concentration of 10 µM to minimize the effects of prolonged toxicity resulting in excessive protein degradation. See Appendix B for a list of all proteins. To be able to easily distinguish between changes in abundance, fold changes are given as logarithmic values to the base of two, where a $\log_2$ fold change (FC) of +1.00 indicates a doubling of protein expression in the uranium-treated sample and an FC value of −1.00 would indicate the control had double the amount of protein than the uranium-treated sample. A q-value less than 0.05 was used to account for false discovery and determine significance between the three replicates of each testing condition (Karp et al., 2007).

Out of the 21 identified proteins directly responsible for CME and vesicular trafficking, only seven showed statistically significant differential expression between uranium-treated and control conditions (Table **1**). One of these was a clathrin light chain variant, which showed an increase in abundance, with an FC value of 0.44. Additionally, there were several clathrin heavy chain variants showing FC values of −0.84, −0.73 and 0.41 with uranium treatment, as well as an EPSIN 2-like protein showing a uranium-induced increase in expression of 0.22 FC units. Another significantly affected protein was a putative clathrin assembly protein showing an FC value of 0.27, albeit having a considerably low confidence score. Aside from these seven

proteins, there were other variants of clathrin heavy and light chains being expressed with no statistically significant differences in the presence of uranium. Other CME-related proteins expressed included clathrin assembly adaptor proteins and proteins guiding vesicular traffic, all showing no significant change in abundance.

One would assume that since clathrin heavy and light chains are mainly responsible for the formation of endocytic vesicles in CME, regardless of cargo and destination, they would both be good indicators for quantifying vesicle uptake. In this light, recent evidence has shown that clathrin heavy chain expression may not be linearly tied to clathrin vesicle formation. Tahara et al. (2007) and Dhonukshe et al. (2007) claim that an overexpression of the clathrin heavy chain leads to an inhibition of endocytosis. This would imply that solely quantifying the abundance of the clathrin light chain, rather than that of both clathrin heavy and light chains, would be a more accurate indicator for changes in the rate of endocytosis, which Wang et al. (2013) and Tahara et al. (2007) also advocate. Therefore, the results in Table **1** would argue that there was no major change in the amount of CME in uranium-exposed BY-2 cells, and if anything, the observed slight increase in clathrin light chain expression would hint towards an increase in endocytosis. Remarkably however, the cells seem to be considerably altering the expression of some heavy chain variants of clathrin, suggesting that a specific heavy chain variant could be involved in heavy-metal-related (or uranium-related) CME.

Table **1**: Relative protein abundances (log_2 fold changes) involved in clathrin-mediated endocytosis comparing tobacco BY-2 cells exposed to 10 µM uranyl(VI) nitrate for 24 h vs. unexposed cells. Statistical significance (*) is denoted by $q \leq 0.05$; TAIR: The Arabidopsis Information Resource.

UniProt Accession	Gene ID	Protein	Functional Description	Description source	Confidence score	Mass (Da)	q Value	Log 2 FC
A0A1S3Z926; A0A1S4B7G0	LOC107784283	clathrin interactor EPSIN 2-like	Transport via clathrin-coated vesicles from the trans-Golgi network to endosomes. Stimulates clathrin assembly.	UniProt	136	97,935	0.02*	0.22
A0A1S4C6G3; A0A1S4ALF5	LOC107815448	clathrin heavy chain	Heavy chain of clathrin coat protein.	UniProt	2838	193,579	0.02*	-0.84
A0A1S3ZLQ4; A0A1S3WZ44	LOC107788165	putative clathrin assembly protein At2g25430	Clathrin coat assembly, clathrin-dependent endocytosis, vesicle budding from membrane	TAIR	47	67,872	0.02*	0.27
A0A1S4D5H1	LOC107826230	clathrin heavy chain	Heavy chain of clathrin coat protein.	UniProt	2540	194,011	0.03*	-0.73
A0A1S3ZY26	LOC107791617	clathrin heavy chain	Heavy chain of clathrin coat protein.	UniProt	2421	193,993	0.04*	0.41
A0A1S3X3V1; A0A1S4C6L6	LOC107760966	clathrin light chain	Light chain of clathrin coat protein.	UniProt	311	35,504	0.04*	0.44
A0A1S3XNB8; A0A1S4BVK7; A0A1S4BJ02; A0A1S4CD03	LOC107767042	AP-2 complex subunit mu-like	Involved in clathrin-dependent endocytosis in which cargo proteins are incorporated into vesicles surrounded by clathrin (clathrin-coated vesicles, CCVs) which are destined for fusion with the early endosome.	UniProt	169	49,781	0.05*	-0.51
A0A1S3XCL3	LOC107763511	clathrin light chain	Light chain of clathrin coat protein.	UniProt	113	29,685	0.08	-0.35

UniProt Accession	Gene ID	Protein	Functional Description	Description source	Confidence score	Mass (Da)	q Value	Log 2 FC
A0A1S4D5T7; A0A1S4DNU5	LOC107826292	AP-2 complex subunit alpha	Involved in clathrin-dependent endocytosis in which cargo proteins are incorporated into vesicles surrounded by clathrin (clathrin-coated vesicles, CCVs) which are destined for fusion with the early endosome.	UniProt	402	114,588	0.09	-0.53
A0A1S4A500; A0A1S4A526; A0A1S4CT74	LOC107793819	clathrin interactor EPSIN 3-like isoform X1	Transport via clathrin-coated vesicles from the trans-Golgi network to endosomes. Stimulates clathrin assembly.	UniProt	105	98,034	0.09	-0.43
A0A1S4C4M9	LOC107815033	clathrin heavy chain 1-like	Heavy chain of clathrin coat protein.	UniProt	2338	134,959	0.13	0.27
A0A1S3YES2	LOC107775474	AP-2 complex subunit alpha	Involved in clathrin-dependent endocytosis in which cargo proteins are incorporated into vesicles surrounded by clathrin (clathrin-coated vesicles, CCVs) which are destined for fusion with the early endosome.	UniProt	382	114,477	0.19	0.34
A0A1S3X3B5; A0A1S4A7M9	LOC107760733	protein TPLATE	Acts in concert with AP2 in endocytosis.	Gadeyne et al., 2014	446	130,702	0.21	-0.12
A0A1S3Z4B7	LOC107782807	putative clathrin assembly protein At5g35200	Vesicle budding from membrane.	TAIR	23	61,151	0.24	-0.20
A0A1S3Z9A1; A0A1S4AXR4	LOC107784340	putative clathrin assembly protein At2g01600	ANTH domain-containing protein which functions as adaptor protein for clathrin-mediated endocytosis (CME) of the secretory vesicle-associated longintype R-SNARE VAMP72 group. Interacts with the SNARE domain of VAMP72 and clathrin at the plasma membrane. Required for recycling of R-SNARE proteins.	TAIR	124	62,887	0.30	-0.05

UniProt Accession	Gene ID	Protein	Functional Description	Description source	Confidence score	Mass (Da)	q Value	Log 2 FC
A0A1S4A121; A0A1S4DR69; A0A1S3XSG8	LOC107792655	AP-2 complex subunit alpha	Involved in clathrin-dependent endocytosis in which cargo proteins are incorporated into vesicles surrounded by clathrin (clathrin-coated vesicles, CCVs) which are destined for fusion with the early endosome.	UniProt	429	115,182	0.32	-0.13
A0A1S4BEG0; A0A1S4DNZ0	LOC107807398	clathrin interactor EPSIN 1-like	Transport via clathrin-coated vesicles from the trans-Golgi network to endosomes. Stimulates clathrin assembly.	UniProt	253	63,993	0.36	-0.02
A0A1S4CC44	LOC107817476	probable clathrin assembly protein At4g32285	Putative clathrin assembly protein, component of TPLATE complex that functions in clathrin-mediated endocytosis.	TAIR	117	48,373	0.37	-0.05
A0A1S4B3W2; A0A1S4BTL4	LOC107804273	clathrin interactor EPSIN 1-like	Transport via clathrin-coated vesicles from the trans-Golgi network to endosomes. Stimulates clathrin assembly.	UniProt	220	59,105	0.39	-0.07
A0A1S4DK63	LOC107830669	clathrin interactor EPSIN 1-like isoform X1	Transport via clathrin-coated vesicles from the trans-Golgi network to endosomes. Stimulates clathrin assembly.	UniProt	242	64,243	0.40	-0.08
A0A1S4ASV3	LOC107801015	clathrin heavy chain 1-like	Heavy chain of clathrin coat protein.	UniProt	1971	147,946	0.40	-0.02

426

3.3. Inhibition of endocytosis leads to reduced uranium bioassociation

To better gauge the contribution of endocytosis to uranium uptake, the total amount of bioassociated uranium was quantified in the presence and absence of the endocytosis blocker, wortmannin. Cells were initially treated with 33 µM wortmannin for 30 min, after which, they were exposed to 20 µM uranyl(VI) nitrate for 6 h. A 6-h exposure was chosen here for two reasons. Firstly, to keep the experimental conditions comparable to the visualization of endocytosis (Fig. 2). Secondly, to cause as little plasma membrane leakage as possible due to uranium-conferred toxicity (Chen et al., 2021), thereby inhibiting the amount of uranium that could move freely into the cell as opposed to uranium taken up by transporters and/or endocytosis. Cells were washed to remove loosely-bound uranium and uranium content was determined in the resulting biomass. The wortmannin and uranium-treated cells exhibited a significant decrease in bioassociated (surface-bound and internalized) uranium compared to uranium-treated cells without wortmannin (Fig. **4**). Thus, an inhibition of endocytosis by wortmannin led to a 14% decrease in bioassociated uranium during 6 h of exposure.

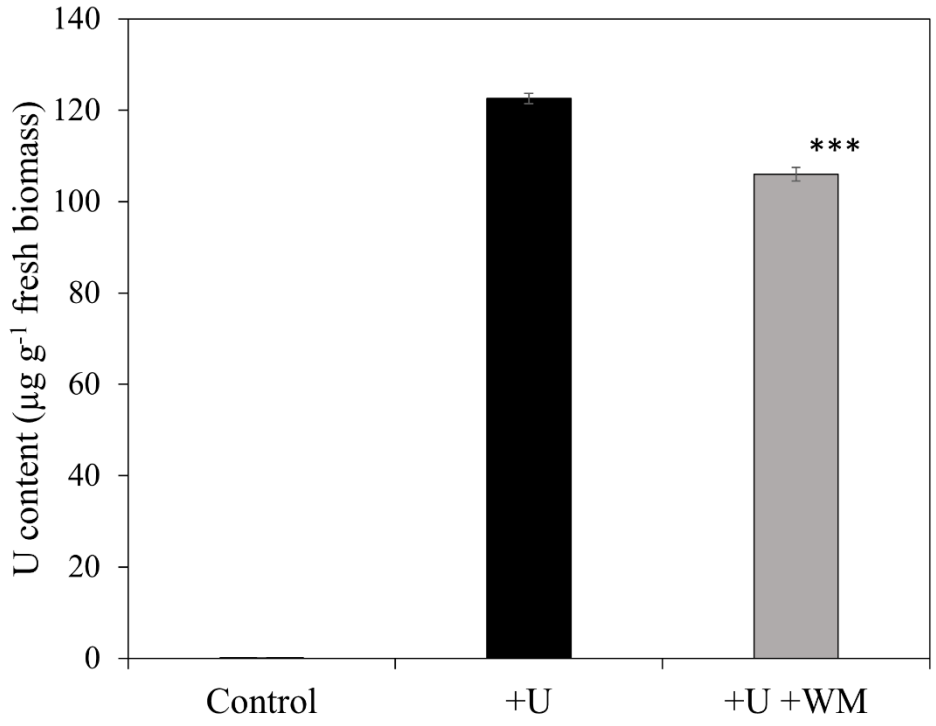

Fig **4**: Uranium bioassociation to untreated BY-2 cells (control), cells treated with 20 µM uranyl(VI) nitrate (+U) and cells treated with both 20 µM uranyl(VI) nitrate and 33 µM wortmannin (+U +WM) for 6 h. Error bars represent standard errors of the mean from three measurements of one biological replicate. *** represents statistical significance between +U and +U+WM where $p < 0.001$.

3.4. Uranium localizes to vacuolar spaces and adsorbs to cell surface components

EDX is an established analytical method based on the fingerprints of an element's X-ray emissions excited by an energetic source, such as an electron beam, and the possibility of coupling EDX measurements in electron microscopy has opened up avenues of research exploring metal interaction with biological systems (Colpan et al., 2018). Hence, TEM and EDX analysis were used to study the localization of uranium in BY-2 cells. Conventional bright-field TEM (Fig. **A.4**) along with STEM-based EDX measurements were performed on BY-2 cells exposed to 20 µM uranium for 24 h. These micrographs revealed a formation of dense needle-like entities in what seem to be vacuolar/late endosomal compartments (Fig. **5a**, **A.5, A.6**). EDX-based spectrum imaging analysis of these objects was performed and evaluation of the emission at 13.612 keV, which is the $L_{\alpha 1}$ peak specific to uranium, showed that they were indeed composed of uranium (Fig. **5b**). Overlaying the EDX maps of the other elements intriguingly showed that the uranium signal distinctly colocalized with two elements in particular, namely, phosphorus and oxygen, which was substantiated by the presence of a white signal (Fig. **5c, A.7a**). Additionally, the uranium signal showed colocalization with those of sulphur and nitrogen (Fig. **5d, A.7b**) but not as densely as with oxygen and phosphorus.

Upon investigation of uranium adsorption to cell surfaces, i.e. the plasma membrane and cell wall, after exposure to 20 µM uranyl(VI) nitrate, there were no uranium signals detected at these cell components. A conceivable explanation for this would be that much of the passively adsorbed uranium was washed away by the TEM preparation process, thus making any adsorbed uranium too little to detect. Therefore, a 24-h exposure to a 10-fold higher concentration of 200 µM uranium was tested. Here, a clear signal was found in defined parts of the cell wall and cell membrane (Fig. **6**). The spectra in Fig. **6** were obtained from selected regions of the electron micrographs containing noticeable quantities of uranium. A reference spectrum was also obtained from an area devoid of uranium (Fig. **A.8**) to make clear the presence of the uranium $L_{\alpha 1}$ peak in areas where it was found. Curiously, the uranium was not ubiquitously distributed along these surfaces as we had anticipated, suggesting an accumulation of specific binding ligands in defined parts of the cell wall and plasma membrane.

469 Furthermore, the same needle-like objects in vacuolar compartments were found in the
470 high-exposure treatment. The formation of vacuolar precipitates in both 20- and 200-µM
471 uranium exposures, which contained a much greater amount of uranium than present at the
472 plasma membrane or cell wall, would suggest an accumulation of uranium in the vacuole and
473 argue for an active uptake mechanism resulting in a deposition of uranium in vacuoles.

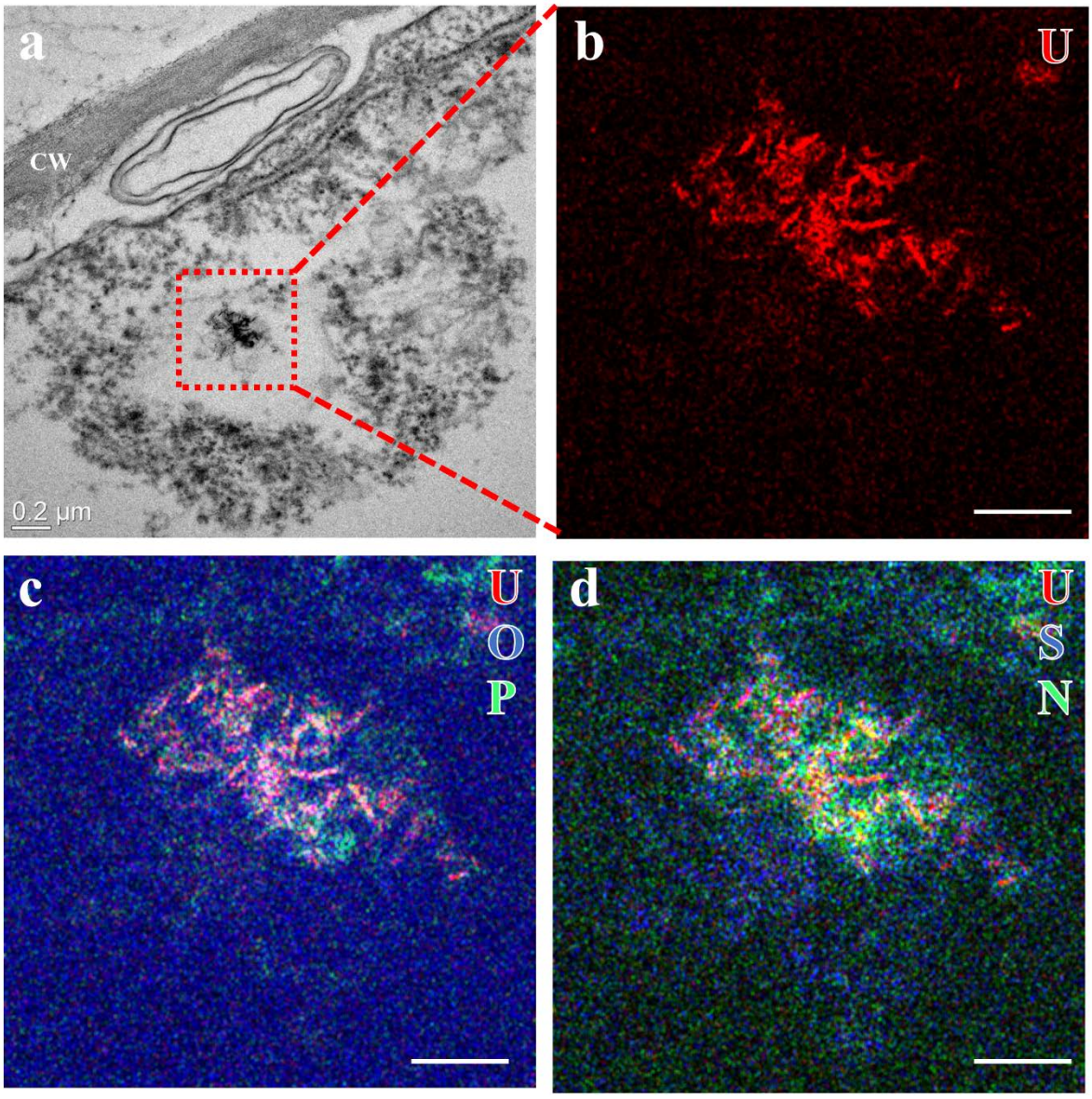

Fig 5: Bright-field transmission electron micrograph (a) of uranium-containing needle-like structures in tobacco BY-2 cells exposed to 20 µM uranyl(VI) nitrate for 24 h. EDX-based elemental mapping (b, c and d) is shown for the structures in a, with c and d containing overlays of various signals. CW: cell wall; N: nitrogen; O: oxygen; P: phosphorus; S: sulphur; U: uranium; scale bar in element distributions: 100 nm.

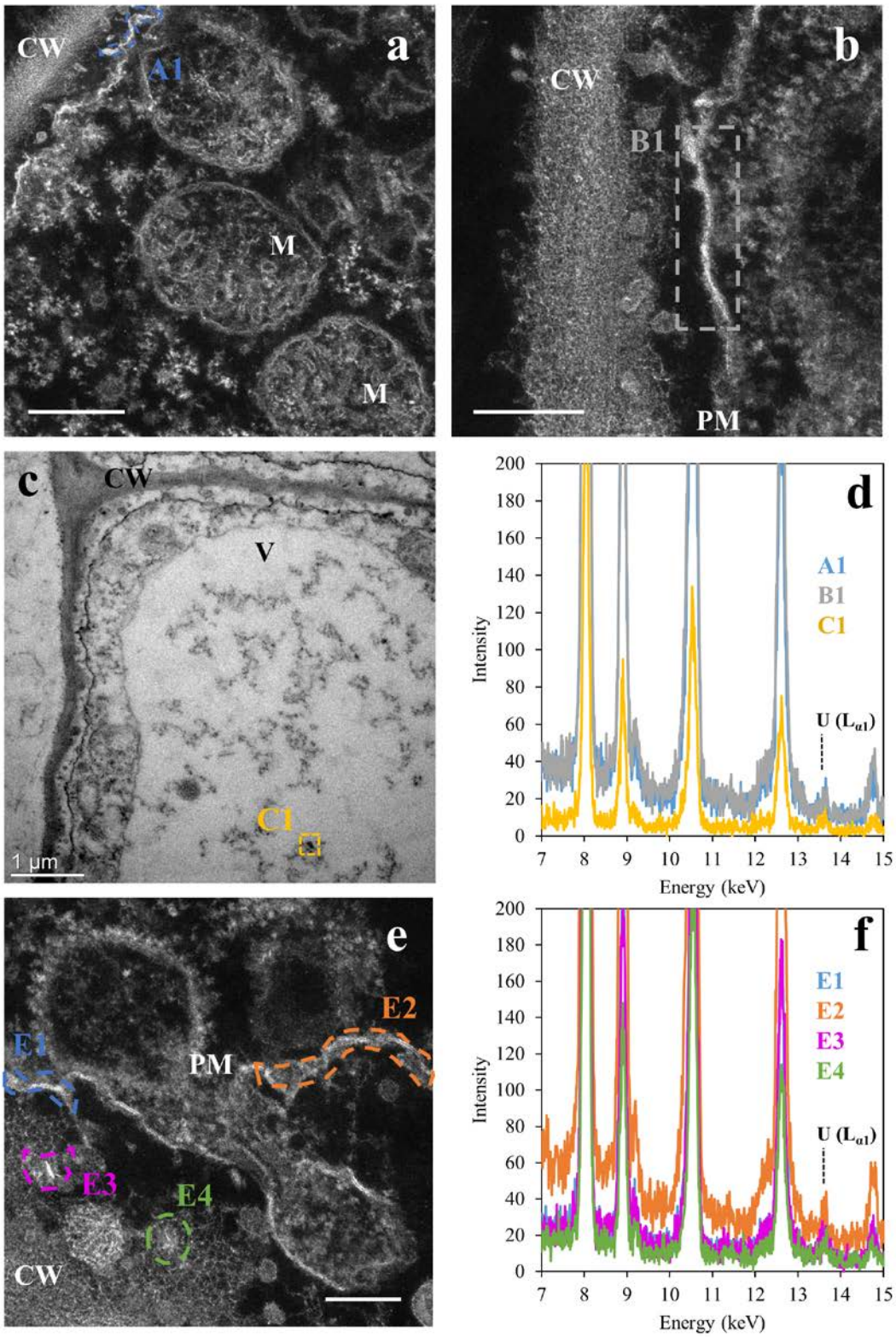

Fig **6**: Uranium adsorption and precipitation in tobacco BY-2 cells exposed to 200 µM uranyl(VI) nitrate for 24 h. EDX sum spectra in panel d are from selected regions in the electron micrographs in a, b and c, labelled A1, B1 and C1, respectively, and the sum spectra from f are from selected regions in panel e, labelled E1-E4, to show the presence of uranium. CW: cell wall; M: mitochondria; PM: plasma membrane; V: vacuole; scale bars: 500 nm in a, 200 nm in b and e. The dotted lines in the spectra of d and f point to the position of the $L_{\alpha 1}$ peak of uranium (13.612 keV).

4. Discussion

4.1. The effect of phosphate deficiency

While transporter-mediated uptake of heavy metals has been extensively investigated and seems to be one of the main modes of metal transport into cells, the endocytic uptake of metals cannot be easily disregarded and should receive more attention, in particular, for non-essential toxic heavy metals. Endocytosis, being an active mode of uptake, requires the use of guanosine-5'-triphosphate (GTP) and therefore requires adequate phosphate reserves within the cell (Gadeyne et al., 2014; Jelínková et al., 2015). Furthermore, vesicular trafficking, which follows the formation of clathrin vesicles, is also guided by a series of Rab-GTPases to ensure that vesicular cargo reach their intended destinations (Nielsen et al., 2008). It was therefore imperative that the BY-2 cells in suspension culture had sufficient access to inorganic phosphate in order to carry out vesicular uptake and trafficking efficiently.

Cell growth and viability experiments proved that cells within 24 h in phosphate-deficient medium showed high viability and vitality, as was seen by an increase in biomass. Since cells would otherwise be arrested in their cell cycle during severe phosphate starvation (Sano et al., 1999), our observations could confirm that a 24-h incubation period in phosphate-deficient medium provided adequately healthy cells for uranium exposure. This would consequently give rise to a more accurate assessment of the cell's response to uranium. Additionally, this would more closely represent a natural encounter with uranium, in contrast to prolonged culture in phosphate deficiency, since whole plants have greater reserves of phosphate, which they are able to mobilize and translocate under low soil phosphate concentrations (Lin et al., 2009; Mimura, 1995).

4.2. The fate of uranium

Studies of uranium interaction in plants are particularly cumbersome due to the many complex and often undesirable interactions of uranium with various constituents of biological experiments, such as phosphate, as well as the multitude of uranyl(VI) complexes that exist in solution and their unique interaction mechanisms with biological entities. This would explain why detailed investigations into uranium-plant interactions on a molecular level are scarce. The experiments described herein have proven that endocytosis is still in play in the presence of uranium and that blocking endocytosis reduces the amount of bioassociated uranium by 14% over the course of 6 h in tobacco BY-2 cells in phosphate-deficient culture. Few other studies investigating metal endocytosis present more than descriptive evidence. Aluminium

internalization is one mechanism that has been explored in greater detail, and this metal has been found to localize to vacuolar compartments within 3 h in meristematic cells and cells in the distal portion of the transition zone in Arabidopsis roots (Illéš et al., 2006). Therefore, the observed localization of uranium in vacuolar spaces within 24 h can also be expected. Nevertheless, it has to once again be stressed that our experiments were conducted with dedifferentiated cells, which might have differing rates and types of endocytosis when compared to various regions of root tissue.

As a plant cell first encounters uranium in solution, it is highly likely that adsorption to the cell wall and plasma membrane would be the fastest and most intense form of bioassociation. This has been observed by Moll et al. (2020) in callus cultures of *Brassica napus*. Various ligands such as phosphate and carboxylic groups from surface proteins, phospholipids and sugar moieties, would be prospective binding partners for metals such as uranium and cause immobilisation at these cell surfaces (Koban and Bernhard, 2007; Krzesłowska, 2011). In former studies involving lead, it has been shown that there is an endocytic uptake of lead deposits on low-methylesterified pectins on the cell wall (Krzesłowska, 2011; Krzesłowska et al., 2010). There was an immobilization of uranium to the cell walls of BY-2 cells (Fig. **6e**), which would thus make plausible a scenario of an endocytic uptake of such cell wall components during cell wall remodelling as a response to heavy metal stress.

In terms of sorption processes, we observed uranium bound not only to the cell wall but also at the plasma membrane. Since endocytosis is still active in the presence of uranium, it could very well be that a considerable amount of plasma-membrane-bound uranium is also internalized. Wheeler & Hanchey (1971) were the first to report the very prominent presence of needle-like crystals in oat roots exposed to uranium and postulated an endocytic uptake of these precipitates. They were however unable to experimentally verify, as they would today, if this was indeed endocytosis. For instance, all heavily contrasted areas of their electron micrographs were automatically assumed to be uranium without any elemental analysis, and vesicles in root tissue were assumed to arise due to endocytosis/pinocytosis, while exocytosis to expel uranium from vacuoles was not considered. Moreover, the concentrations of uranium they used were far higher (1 mM) than what would be environmentally relevant. Unlike in their study, we did not observe the formation of such crystals at cell surfaces, instead only saw trace amounts and uranium localized in pockets along the membrane. Modern spectroscopy techniques using EDX (including our own analyses) have now shown that these crystals are

mostly comprised of uranyl(VI) phosphate (Jessat et al., 2021; Laurette et al., 2012; Rodriguez-Freire et al., 2021). The excessive formation of crystals in their study could be best explained by the immediate transfer of their roots from a phosphate-rich environment into highly concentrated uranyl(VI) acetate solutions, which would cause uranium to precipitate in the form of uranyl(VI) phosphate complexes with a needle-like appearance. The presence of such crystals, caused by the high artificial phosphate concentrations generally not observed in soil, could lead to a wholly different tissue response that what the plant would undergo when in moderately uranium-contaminated soil, where crystals do not exist in such abundance. This could be in the form of triggering or inhibiting endocytosis since vesicle uptake is also dependent on the cargo stimulus (Reynolds et al., 2018). Nevertheless, considering the observations in their study and in ours, we are now able to confirm an endocytic uptake of uranium at environmentally relevant exposure levels.

Many studies involving uranium-exposed plant tissue have consistently discovered the formation of needle-like precipitates, in what appear to be vacuolar and late-endosomal compartments of salt cedar plants (Rodriguez-Freire et al., 2021) and suspension cultures of rapeseed (Jessat et al., 2021). Compared to those studies, we used five-fold lower uranium exposure levels (20 µM), albeit, with dedifferentiated suspension cultures instead of tissue, and still observed an accumulation of these precipitates. This would suggest that, one, uranium is actively targeted to the vacuole for sequestration, and two, this is a likely scenario for most plant cell types. The colocalization of the uranium signal with four other EDX signals, namely, phosphorus, oxygen, sulphur and nitrogen, showed that these were not simply precipitates of uranyl(VI) phosphate. The presence of sulphur and nitrogen point to thiol-based chelation mechanisms. Uranium is known to induce cellular production of glutathione (Lai et al., 2021; Viehweger et al., 2011), for instance, which could bind to uranium as it enters the cell, preventing its interaction with susceptible biomolecules, and end up in the vacuole as uranium-glutathione chelates.

It is difficult to say how much of this vacuole sequestration is a result of endocytosis and vesicle trafficking, as opposed to transporter-based mechanisms. There is already evidence for a transporter-mediated uptake of uranium into BY-2 cells (Rajabi et al., 2021; Sarthou et al., 2022), however, an endocytic uptake of the metal would provide a completely different pathway as opposed to one that is transporter-mediated. It would provide greater control over where the metal is compartmentalized, as opposed to freely loading metal into the cytosol, thereby reducing contact with susceptible biomolecules. One of the main roles of endocytosis

is receptor recycling for plasma membrane remodelling, which involves changing the proteins being expressed on the plasma membrane to adapt to a specific situation. This would help the cell to cope in the presence of toxic metals, by removing proteins on the membrane, which might inadvertently cause metal transport into the cell, and replacing them with such as are needed to prevent and combat the effects of metal toxicity (De Caroli et al., 2020; Wang et al., 2020). The removed proteins would subsequently be targeted initially to multi-vesicular bodies (or endosomes) and eventually to the vacuole for degradation.

Thus, one could imagine that endocytosed uranium would be trafficked to the vacuole as part of the receptor recycling process. The question remains as to whether the cell does this intentionally or whether it is an unintended effect of receptor recycling and protein degradation. An unintentional uptake of uranium could stem from autophagy-driven events, for instance, which are known to also be linked to endocytosis (Birgisdottir and Johansen, 2020). The stress conferred to these cells by the presence of the radionuclide could initiate autophagy in an effort to recycle damaged proteins as a result of oxidative stress and would therefore promote events of endocytosis as well (Hasan et al., 2017).

An intentional uptake would likely involve a change in binding ligands on the plasma membrane to cause as much adsorption of the toxic metal, followed then by vesicular uptake and sequestration in the vacuole. There are two pieces of evidence presented in this study that would argue for this. One, there is a change in the expression of clathrin heavy chain variants in the presence of uranium, suggesting that there is a shift in the type of endocytosis taking place in terms of cargo and destination, and two, uranium is not evenly distributed along the plasma membrane but concentrated in pockets, alluding to clusters of uranium-ligand complexes. Although these observations could very well imply an intentional vesicular uptake and sequestration of the metal, more thorough investigation is needed to confirm this.

5. Conclusions and outlook

The herein described results present a case for endocytosis as an uptake mechanism of uranium into plant cells along with its trafficking to and storage in vacuolar compartments. The successful implementation of a plant cell culture in temporary phosphate deficiency has now made it possible to tackle important research questions, not only studying uranium interaction but also interaction with other relevant metals. As a result, we could conclude that endocytosis remains active in the presence of uranium, contributing to 14% of the bioassociated uranium, and there was significant deposition of uranium precipitates in the vacuole. The phenomenon of uranium adsorption to cell surfaces (cell wall and plasma membrane) was clearly visually demonstrated for the first time despite being observed more than 30 years back and remained unverified until now (Wheeler and Hanchey, 1971). These observations bring us a step closer to elucidating mechanisms of radionuclide uptake in plants, which have remained long elusive. Nevertheless, some questions remain that are yet to be answered. Are there similar levels of uranium endocytosis in specialized plant tissue? Does endocytosis contribute more than transporter-based mechanisms towards uranium uptake from the rhizosphere? Does the vacuole remain the final resting place for sequestered uranium in BY-2 cells or are there mechanisms of exudation at play?

A clearer understanding of these events would greatly advance strategies for nuclear risk assessment and phytoremediation, especially since there are many biological aspects and factors that are yet to be considered in modelling studies involving radionuclide uptake. These results verify the uptake of uranium into plant cells via endocytosis, thereby consolidating the evidence for non-transporter mediated metal uptake, hence underscoring the importance of investigating the role of endocytosis in the uptake of radionuclides such as uranium.

6. References

Altman, D.G., Bland, M.J., 2005. Standard deviations and standard errors. BMJ 331, 903. https://doi.org/10.1136/bmj.331.7521.903

Andresen, E., Peiter, E., Küpper, H., 2018. Trace metal metabolism in plants. J. Exp. Bot. 69, 909–954. https://doi.org/10.1093/jxb/erx465

Arunakumara, K.K.I.U., Zhang, X., 2007. Heavy metal bioaccumulation and toxicity with special reference to microalgae. J. Ocean Univ. China 7, 60–64. https://doi.org/10.1007/s11802-008-0060-y

Ben, Y., Cheng, M., Wang, L., Zhou, Q., Yang, Z., Huang, X., 2021. Low-dose lanthanum activates endocytosis, aggravating accumulation of lanthanum or/and lead and disrupting homeostasis of essential elements in the leaf cells of four edible plants. Ecotoxicol. Environ. Saf. 221, 112429. https://doi.org/10.1016/j.ecoenv.2021.112429

Berthet, S., Villiers, F., Alban, C., Serre, N.B.C., Martin-Laffon, J., Figuet, S., Boisson, A.M., Bligny, R., Kuntz, M., Finazzi, G., Ravanel, S., Bourguignon, J., 2018. *Arabidopsis thaliana* plants challenged with uranium reveal new insights into iron and phosphate homeostasis. New Phytol. 217, 657–670. https://doi.org/10.1111/nph.14865

Birgisdottir, Å.B., Johansen, T., 2020. Autophagy and endocytosis – interconnections and interdependencies. J. Cell Sci. 133, 228114. https://doi.org/10.1242/jcs.228114

Bolte, S., Talbot, C., Boutte, Y., Catrice, O., Read, N.D., Satiat-Jeunemaitre, B., 2004. FM-dyes as experimental probes for dissecting vesicle trafficking in living plant cells. J. Microsc. 214, 159–173. https://doi.org/10.1111/j.0022-2720.2004.01348.x

Chen, L., Liu, J., Zhang, W., Zhou, J., Luo, D., Li, Z., 2021. Uranium (U) source, speciation, uptake, toxicity and bioremediation strategies in soil-plant system: A review. J. Hazard. Mater. 413, 125319. https://doi.org/10.1016/j.jhazmat.2021.125319

Colpan, C.O., Nalbant, Y., Ercelik, M., 2018. Fundamentals of fuel cell technologies, in: Dincer, I. (Ed.), Comprehensive Energy Systems. Elsevier Inc., pp. 1107–1130. https://doi.org/10.1016/B978-0-12-809597-3.00446-6

Craft, E.S., Abu-Qare, A.W., Flaherty, M.M., Garofolo, M.C., Rincavage, H.L., Abou-Donia, M.B., 2004. Depleted and natural uranium: Chemistry and toxicological effects. J.

649 Toxicol. Environ. Heal. - Part B Crit. Rev. 7, 297–317.
650 https://doi.org/10.1080/10937400490452714

651 De Caroli, M., Furini, A., DalCorso, G., Rojas, M., Di Sansebastiano, G. Pietro, 2020.
652 Endomembrane reorganization induced by heavy metals. Plants 9, 482.
653 https://doi.org/10.3390/plants9040482

654 Dhonukshe, P., Aniento, F., Hwang, I., Robinson, D.G., Mravec, J., Stierhof, Y.D., Friml, J.,
655 2007. Clathrin-mediated constitutive rndocytosis of PIN auxin efflux carriers in
656 Arabidopsis. Curr. Biol. 17, 520–527. https://doi.org/10.1016/j.cub.2007.01.052

657 Doustaly, F., Combes, F., Fiévet, J.B., Berthet, S., Hugouvieux, V., Bastien, O., Aranjuelo, I.,
658 Leonhardt, N., Rivasseau, C., Carrière, M., Vavasseur, A., Renou, J.P., Vandenbrouck,
659 Y., Bourguignon, J., 2014. Uranium perturbs signaling and iron uptake response in
660 *Arabidopsis thaliana* roots. Metallomics 6, 809–821. https://doi.org/10.1039/c4mt00005f

661 Dragwidge, J.M., van Damme, D., 2020. Visualising endocytosis in plants: past, present, and
662 future. J. Microsc. 280, 104–110. https://doi.org/10.1111/jmi.12926

663 Ebbs, S.D., Brady, D.J., Kochian, L. V., 1998. Role of uranium speciation in the uptake and
664 translocation of uranium by plants. J. Exp. Bot. 49, 1183–1190.
665 https://doi.org/10.1093/jxb/49.324.1183

666 Ebbs, S.D., Brady, D.J., Norvell, W.A., Kochian, L. V., 2000. Uranium speciation, plant
667 uptake, and phytoremediation, in: National Conference on Environmental and Pipeline
668 Engineering. pp. 466–475. https://doi.org/10.1061/40507(282)51

669 Ekanayake, G., LaMontagne, E.D., Heese, A., 2019. Never walk alone: clathrin-coated vesicle
670 (CCV) components in plant immunity. Annu. Rev. Phytopathol. 57, 387–409.
671 https://doi.org/10.1146/annurev-phyto-080417-045841

672 Fan, J.L., Wei, X.Z., Wan, L.C., Zhang, L.Y., Zhao, X.Q., Liu, W.Z., Hao, H.Q., Zhang, H.Y.,
673 2011. Disarrangement of actin filaments and Ca^{2+} gradient by $CdCl_2$ alters cell wall
674 construction in *Arabidopsis thaliana* root hairs by inhibiting vesicular trafficking. J. Plant
675 Physiol. 168, 1157–1167. https://doi.org/10.1016/j.jplph.2011.01.031

676 Fujimoto, M., Ueda, T., 2012. Conserved and plant-unique mechanisms regulating plant post-
677 Golgi traffic. Front. Plant Sci. 3, 197. https://doi.org/10.3389/fpls.2012.00197

678 Gadeyne, A., Sánchez-Rodríguez, C., Vanneste, S., Di Rubbo, S., Zauber, H., Vanneste, K.,

679 Van Leene, J., De Winne, N., Eeckhout, D., Persiau, G., Van De Slijke, E., Cannoot, B.,
680 Vercruysse, L., Mayers, J.R., Adamowski, M., Kania, U., Ehrlich, M., Schweighofer, A.,
681 Ketelaar, T., Maere, S., Bednarek, S.Y., Friml, J., Gevaert, K., Witters, E., Russinova, E.,
682 Persson, S., De Jaeger, G., Van Damme, D., 2014. The TPLATE adaptor complex drives
683 clathrin-mediated endocytosis in plants. Cell 156, 691–704.
684 https://doi.org/10.1016/j.cell.2014.01.039

685 Gorman-Lewis, D., Shvareva, T., Kubatko, K.A., Burns, P.C., Wellman, D.M., McNamara, B.,
686 Szymanowski, J.E.S., Navrotsky, A., Fein, J.B., 2009. Thermodynamic properties of
687 autunite, uranyl hydrogen phosphate, and uranyl orthophosphate from solubility and
688 calorimetric measurements. Environ. Sci. Technol. 43, 7416–7422.
689 https://doi.org/10.1021/es9012933

690 Gupta, Dharmendra K., Chatterjee, S., Mitra, A., Voronina, A., Walther, Clemens, 2020.
691 Uranium and plants: elemental translocation and phytoremediation approaches, in: Gupta,
692 D. K., Walther, C. (Eds.), Uranium in Plants and the Environment. Springer Nature
693 Switzerland AG, pp. 149–161. https://doi.org/10.1007/978-3-030-14961-1_7

694 Hasan, M.K., Cheng, Y., Kanwar, M.K., Chu, X.Y., Ahammed, G.J., Qi, Z.Y., 2017. Responses
695 of plant proteins to heavy metal stress—a review. Front. Plant Sci. 8, 1492.
696 https://doi.org/10.3389/fpls.2017.01492

697 Hiraga, A., Kaneta, T., Sato, Y., Sato, S., 2010. Programmed cell death of tobacco BY-2 cells
698 induced by still culture conditions is affected by the age of the culture under agitation.
699 Cell Biol. Int. 34, 189–196. https://doi.org/10.1042/cbi20090003

700 Hübner, R., Depta, H., Robinson, D.G., 1985. Endocytosis in maize root cap cells - Evidence
701 obtained using heavy metal salt solutions. Protoplasma 129, 214–222.
702 https://doi.org/10.1007/BF01279918

703 Illéš, P., Schlicht, M., Pavlovkin, J., Lichtscheidl, I., Baluška, F., Ovečka, M., 2006.
704 Aluminium toxicity in plants: Internalization of aluminium into cells of the transition zone
705 in Arabidopsis root apices related to changes in plasma membrane potential, endosomal
706 behaviour, and nitric oxide production. J. Exp. Bot. 57, 4201–4213.
707 https://doi.org/10.1093/jxb/erl197

708 Jelínková, A., Müller, K., Fílová-Parezová, M., Petrášek, J., 2015. NtGNL1a ARF-GEF acts in
709 endocytosis in tobacco cells. BMC Plant Biol. 15, 272. https://doi.org/10.1186/s12870-

710 015-0621-3

711 Jeong, J., Connolly, E.L., 2009. Iron uptake mechanisms in plants: Functions of the FRO family
712 of ferric reductases. Plant Sci. 176, 709–714.
713 https://doi.org/10.1016/j.plantsci.2009.02.011

714 Jessat, J., Sachs, S., Moll, H., John, W., Steudtner, R., Hübner, R., Bok, F., Stumpf, T., 2021.
715 Bioassociation of U(VI) and Eu(III) by plant (*Brassica napus*) suspension cell cultures -
716 a spectroscopic investigation. Environ. Sci. Technol. 55, 6718–6728.
717 https://doi.org/10.1021/acs.est.0c05881

718 Karp, N.A., McCormick, P.S., Russell, M.R., Lilley, K.S., 2007. Experimental and statistical
719 considerations to avoid false conclusions in proteomics studies using differential in-gel
720 electophoresis. Mol. Cell. Proteomics 6.8, 1354–1364.
721 https://doi.org/10.1074/mcp.M600274-MCP200

722 Koban, A., Bernhard, G., 2007. Uranium(VI) complexes with phospholipid model compounds
723 - A laser spectroscopic study. J. Inorg. Biochem. 101, 750–757.
724 https://doi.org/10.1016/j.jinorgbio.2007.01.001

725 Krzesłowska, M., 2011. The cell wall in plant cell response to trace metals: Polysaccharide
726 remodeling and its role in defense strategy. Acta Physiol. Plant.
727 https://doi.org/10.1007/s11738-010-0581-z

728 Krzesłowska, M., Lenartowska, M., Samardakiewicz, S., Bilski, H., Woźny, A., 2010. Lead
729 deposited in the cell wall of *Funaria hygrometrica* protonemata is not stable - A
730 remobilization can occur. Environ. Pollut. 158, 325–338.
731 https://doi.org/10.1016/j.envpol.2009.06.035

732 Lai, J., Liu, Z., Li, C., Luo, X., 2021. Analysis of accumulation and phytotoxicity mechanism
733 of uranium and cadmium in two sweet potato cultivars. J. Hazard. Mater. 409, 124997.
734 https://doi.org/10.1016/j.jhazmat.2020.124997

735 Laing, W., Christeller, J., 2004. Extraction of proteins from plant tissues. Curr. Protoc. protein
736 Sci. 38, 4.7.1-4.7.7. https://doi.org/10.1002/0471140864.ps0407s38

737 Langmuir, D., 1978. Uranium solution-mineral equilibria at low temperatures with applications
738 to sedimentary ore deposits. Geochim. Cosmochim. Acta 42, 547–569.
739 https://doi.org/10.1016/0016-7037(78)90001-7

Laroche, L., Henner, P., Camilleri, V., Morello, M., Garnier-Laplace, J., 2005. Root uptake of uranium by a higher plant model (*Phaseolus vulgaris*) – bioavailability from soil solution. Radioprotection 40, S33–S39. https://doi.org/10.1051/radiopro

Laurette, J., Larue, C., Llorens, I., Jaillard, D., Jouneau, P.H., Bourguignon, J., Carrière, M., 2012. Speciation of uranium in plants upon root accumulation and root-to-shoot translocation: A XAS and TEM study. Environ. Exp. Bot. 77, 87–95. https://doi.org/10.1016/j.envexpbot.2011.11.005

Lin, W.-Y., Lin, S.-I., Chiou, T.-J., 2009. Molecular regulators of phosphate homeostasis in plants. J. Exp. Bot. 60, 1427–1438. https://doi.org/10.1093/jxb/ern303

Majovsky, P., Naumann, C., Lee, C.W., Lassowskat, I., Trujillo, M., Dissmeyer, N., Hoehenwarter, W., 2014. Targeted proteomics analysis of protein degradation in plant signaling on an LTQ-Orbitrap mass spectrometer. J. Proteome Res. 13, 4246–4258. https://doi.org/10.1021/pr500164j

Mimura, T., 1995. Homeostasis and transport of inorganic phosphate in plants. Plant Cell Physiol. 36, 1–7. https://doi.org/10.1093/oxfordjournals.pcp.a078724

Moll, H., Sachs, S., Geipel, G., 2020. Plant cell (*Brassica napus*) response to europium(III) and uranium(VI) exposure. Environ. Sci. Pollut. Res. 27, 32048–32061. https://doi.org/10.1007/s11356-020-09525-2

Mulisch, M., Welsch, U., 2010. Romeis Mikroskopische Technik, 18th ed. Spektrum Akademischer Verlag, Heidelberg.

Murphy, A.S., Bandyopadhyay, A., Holstein, S.E., Peer, W.A., 2005. Endocytotic cycling of PM proteins. Annu. Rev. Plant Biol. 56, 221–251. https://doi.org/10.1146/annurev.arplant.56.032604.144150

Nagata, T., Nemoto, Y., Hasezawa, S., 1992. Tobacco BY-2 Cell Line as the “HeLa” Cell in the Cell Biology of Higher Plants. Int. Rev. Cytol. 132, 1–30. https://doi.org/10.1016/S0074-7696(08)62452-3

Neill, T.S., Morris, K., Pearce, C.I., Sherriff, N.K., Burke, M.G., Chater, P.A., Janssen, A., Natrajan, L., Shaw, S., 2018. Stability, composition, and core-shell particle structure of uranium(IV)-silicate colloids. Environ. Sci. Technol. 52, 9118–9127. https://doi.org/10.1021/acs.est.8b01756

Nicholas, D.J.D., 1975. The functions of trace elements in planta, in: Nicholas, D.J.D., Egan, A.H. (Eds.), Trace Elements in Soil-Plant-Animal Systems. pp. 181–198. https://doi.org/10.1016/B978-0-12-518150-1.X5001-0

Nielsen, E., Cheung, A.Y., Ueda, T., 2008. The regulatory RAB and ARF GTPases for vesicular trafficking. Plant Physiol. 147, 1516–1526. https://doi.org/10.1104/pp.108.121798

Nishida, S., Tsuzuki, C., Kato, A., Aisu, A., Yoshida, J., Mizuno, T., 2011. AtIRT1, the primary iron uptake transporter in the root, mediates excess nickel accumulation in *Arabidopsis thaliana*. Plant Cell Physiol. 52, 1433–1442. https://doi.org/10.1093/pcp/pcr089

Orsburn, B.C., 2021. Proteome discoverer-a community enhanced data processing suite for protein informatics. Proteomes 9, 15. https://doi.org/10.3390/proteomes9010015

Pérez-Gómez, J., Moore, I., 2007. Plant endocytosis: it is clathrin after all. Curr. Biol. 17, R217-219. https://doi.org/10.1016/j.cub.2007.01.045

Perez-Riverol, Y., Csordas, A., Bai, J., Bernal-Llinares, M., Hewapathirana, S., Kundu, D.J., Inuganti, A., Griss, J., Mayer, G., Eisenacher, M., Pérez, E., Uszkoreit, J., Pfeuffer, J., Sachsenberg, T., Yilmaz, Ş., Tiwary, S., Cox, J., Audain, E., Walzer, M., Jarnuczak, A.F., Ternent, T., Brazma, A., Vizcaíno, J.A., 2019. The PRIDE database and related tools and resources in 2019: Improving support for quantification data. Nucleic Acids Res. 47, D442–D450. https://doi.org/10.1093/nar/gky1106

Rajabi, F., Jessat, J., Garimella, J.N., Bok, F., Steudtner, R., Stumpf, T., Sachs, S., 2021. Uranium(VI) toxicity in tobacco BY-2 cell suspension culture – A physiological study. Ecotoxicol. Environ. Saf. 211, 111883. https://doi.org/10.1016/j.ecoenv.2020.111883

Raskin, I., Kumar, P.N., Dushenkov, S., Salt, D.E., 1994. Bioconcentration of heavy metals by plants. Curr. Opin. Biotechnol. 5, 285–290. https://doi.org/10.1016/0958-1669(94)90030-2

Ratnikov, A.N., Sviridenko, D.G., Popova, G.I., Sanzharova, N.I., Mikailova, R.A., 2020. The behaviour of uranium in soils and the mechanisms of its accumulation by agricultural plant, in: Gupta, D.K., Walther, C. (Eds.), Uranium in Plants and the Environment. Springer Nature Switzerland AG, pp. 113–135. https://doi.org/10.1007/978-3-030-14961-1_5

Rehman, M.Z., Rizwan, M., Sohail, M.I., Ali, S., Waris, A.A., Khalid, H., Naeem, A., Ahmad, H.R., Rauf, A., 2019. Opportunities and challenges in the remediation of metal-contaminated soils by using tobacco (*Nicotiana tabacum* L.): a critical review. Environ. Sci. Pollut. Res. 26, 18053–18070. https://doi.org/10.1007/s11356-019-05391-9

Reynolds, E.S., 1963. The use of lead citrate at high pH as an electron-opaque stain in electron microscopy. J. Cell Biol. 17, 208–212. https://doi.org/10.1083/jcb.17.1.208

Reynolds, G.D., Wang, C., Pan, J., Bednarek, S.Y., 2018. Inroads into internalization: Five years of endocytic exploration. Plant Physiol. 176, 208–218. https://doi.org/10.1104/pp.17.01117

Ribera, D., Labrot, F., Tisnerat, G., Narbonne, J.F., 1996. Uranium in the environment: occurrence, transfer, and biological effects. Rev. Environ. Contam. Toxicol. 146, 53–89. https://doi.org/10.1007/978-1-4613-8478-6_3

Rigal, A., Doyle, S.M., Robert, S., 2015. Live cell imaging of FM4-64, a tool for tracing the endocytic pathways in Arabidopsis root cells, in: Estevez, J.M. (Ed.), Plant Cell Expansion: Methods in Molecular Biology (Methods and Protocols). Humana Press, New York, pp. 93–103. https://doi.org/10.1007/978-1-4939-1902-4_9

Rodriguez-Freire, L., DeVore, C.L., El Hayek, E., Berti, D., Ali, A.-M.S., Lezama Pacheco, J.S., Blake, J.M., Spilde, M.N., Brearley, A.J., Artyushkova, K., Cerrato, J.M., 2021. Emerging investigator series: entrapment of uranium–phosphorus nanocrystals inside root cells of *Tamarix* plants from a mine waste site. Environ. Sci. Process. Impacts 23, 73–85. https://doi.org/10.1039/d0em00306a

Rohde, F., Braumann, U.-D., Schmidt, M., 2020. Correlia: an ImageJ plug-in to co-register and visualise multimodal correlative micrographs. J. Microsc. 280, 3–11. https://doi.org/10.1111/jmi.12928

Saenen, E., Horemans, N., Vanhoudt, N., Vandenhove, H., Biermans, G., Van Hees, M., Wannijn, J., Vangronsveld, J., Cuypers, A., 2013. Effects of pH on uranium uptake and oxidative stress responses induced in *Arabidopsis thaliana*. Environ. Toxicol. Chem. 32, 2125–2133. https://doi.org/10.1002/etc.2290

Sano, T., Kuraya, Y., Amino, S., Nagata, T., 1999. Phosphate as a limiting factor for the cell division of tobacco BY-2 Cells. Plant Cell Physiol. 40, 1–8.

https://doi.org/10.1093/oxfordjournals.pcp.a029464

Sarthou, M.C.M., Devime, F., Baggio, C., Figuet, S., Alban, C., Bourguignon, J., Ravanel, S., 2022. Calcium-permeable cation channels are involved in uranium uptake in *Arabidopsis thaliana*. J. Hazard. Mater. 424, 127436. https://doi.org/10.1016/j.jhazmat.2021.127436

Schnug, E., Lottermoser, B.G., 2013. Fertilizer-derived uranium and its threat to human health. Environ. Sci. Technol. 47, 2433–2434. https://doi.org/10.1021/es4002357

Shahandeh, H., Hossner, L.R., 2002. Role of soil properties in phytoaccumulation of uranium. Water. Air. Soil Pollut. 141, 165–180. https://doi.org/10.1023/A:1021346828490

Song, Y., Jin, L., Wang, X., 2017. Cadmium absorption and transportation pathways in plants. Int. J. Phytoremediation 19, 133–141. https://doi.org/10.1080/15226514.2016.1207598

Soudek, P., Petrová, Š., Buzek, M., Lhotský, O., Vaněk, T., 2014. Uranium uptake in *Nicotiana* sp. under hydroponic conditions. J. Geochemical Explor. 142, 130–137. https://doi.org/10.1016/j.gexplo.2013.10.001

Spurr, A.R., 1969. A low-viscosity epoxy resin embedding medium for electron microscopy. J. Ultrastruct. Res. 26, 31–43. https://doi.org/https://doi.org/10.1016/S0022-5320(69)90033-1

Srba, M., Černíková, A., Opatrný, Z., Fischer, L., 2016. Practical guidelines for the characterization of tobacco BY-2 cell lines. Biol. Plant. 60, 13–24. https://doi.org/10.1007/s10535-015-0573-3

Stojanović, M.D., Mihajlović, M.L., Milojković, J. V., Lopičić, Z.R., Adamović, M., Stanković, S., 2012. Efficient phytoremediation of uranium mine tailings by tobacco. Environ. Chem. Lett. 10, 377–381. https://doi.org/10.1007/s10311-012-0362-6

Tahara, H., Yokota, E., Igarashi, H., Orii, H., Yao, M., Sonobe, S., Hashimoto, T., Hussey, P.J., Shimmen, T., 2007. Clathrin is involved in organization of mitotic spindle and phragmoplast as well as in endocytosis in tobacco cell cultures. Protoplasma 230, 1–11. https://doi.org/10.1007/s00709-006-0226-7

Vandenhove, H., 2002. European sites contaminated by residues from the ore-extracting and -processing industries. Int. Congr. Ser. 1225, 307–315. https://doi.org/10.1016/S0531-5131(01)00525-8

Viehweger, K., Geipel, G., 2010. Uranium accumulation and tolerance in *Arabidopsis halleri* under native versus hydroponic conditions. Environ. Exp. Bot. 69, 39–46. https://doi.org/10.1016/j.envexpbot.2010.03.001

Viehweger, K., Geipel, G., Bernhard, G., 2011. Impact of uranium (U) on the cellular glutathione pool and resultant consequences for the redox status of U. BioMetals 24, 1197–1204. https://doi.org/10.1007/s10534-011-9478-6

Wall, J.D., Krumholz, L.R., 2006. Uranium reduction. Annu. Rev. Microbiol. 60, 149–166. https://doi.org/10.1146/annurev.micro.59.030804.121357

Wang, C., Yan, X., Chen, Q., Jiang, N., Fu, W., Ma, B., Liu, J., Li, C., Bednarek, S.Y., Pan, J., 2013. Clathrin light chains regulate clathrin-mediated trafficking, auxin signaling, and development in Arabidopsis. Plant Cell 25, 499–516. https://doi.org/10.1105/tpc.112.108373

Wang, L., Li, J., Zhou, Q., Yang, G., Ding, X.L., Li, X., Cai, C.X., Zhang, Z., Wei, H.Y., Lu, T.H., Deng, X.W., Huang, X.H., 2014. Rare earth elements activate endocytosis in plant cells. Proc. Natl. Acad. Sci. U. S. A. 111, 12936–12941. https://doi.org/10.1073/pnas.1413376111

Wang, X., Gao, Y., Feng, Y., Li, X., Wei, Q., Sheng, X., 2014. Cadmium stress disrupts the endomembrane organelles and endocytosis during *Picea wilsonii* pollen germination and tube growth. PLoS One 9, e94721. https://doi.org/10.1371/journal.pone.0094721

Wang, X., Xu, M., Gao, C., Zeng, Y., Cui, Y., Shen, W., Jiang, L., 2020. The roles of endomembrane trafficking in plant abiotic stress responses. J. Integr. Plant Biol. 62, 55–69. https://doi.org/10.1111/jipb.12895

Wetterlind, J., Richer De Forges, A.C., Nicoullaud, B., Arrouays, D., 2012. Changes in uranium and thorium contents in topsoil after long-term phosphorus fertilizer application. Soil Use Manag. 28, 101–107. https://doi.org/10.1111/j.1475-2743.2011.00376.x

Wheeler, H., Hanchey, P., 1971. Pinocytosis and membrane dilation in uranyl-treated plant roots. Science (80-.). 171, 68–71. https://doi.org/10.1126/science.171.3966.68

Wu, D., Shen, H., Yokawa, K., Baluška, F., 2015. Overexpressing OsPIN2 enhances aluminium internalization by elevating vesicular trafficking in rice root apex. J. Exp. Bot. 66, 6791–6801. https://doi.org/10.1093/jxb/erv385

889 Zavala-Guevara, I.P., Ortega-Romero, M.S., Narváez-Morales, J., Jacobo-Estrada, T.L., Lee,
890 W.K., Arreola-Mendoza, L., Thévenod, F., Barbier, O.C., 2021. Increased endocytosis of
891 cadmium-metallothionein through the 24p3 receptor in an in vivo model with reduced
892 proximal tubular activity. Int. J. Mol. Sci. 22, 7262. https://doi.org/10.3390/ijms22147262

7. Acknowledgments

The first batch of BY-2 cells was kindly provided by Prof. P. Nick from the Botanical Institute, Karlsruhe Institute of Technology. The authors are also grateful for experimental assistance from S. Beutner and S. Bachmann with respect to ICP-MS measurements, and J. Seibt for cell culture. The authors also thank Dr. F. Rajabi for her insight and contributions to wortmannin treatment of BY-2 cells. The use of the Ion Beam Center TEM facilities and the funding of TEM Talos by the German Federal Ministry of Education and Research (BMBF, Grant No. 03SF0451) in the framework of HEMCP are gratefully acknowledged. This work is part of the project TRANS-LARA, which was funded by the BMBF under contract number 02NUK051B.

8. Author contributions

Warren John: conceptualization, data curation, investigation, methodology, validation, visualization, writing – original draft.

Benita Lückel: investigation, methodology, writing – review & editing.

Nicole Matschiavelli: conceptualization, investigation, methodology, writing – review & editing.

René Hübner: formal analysis, investigation, methodology, visualization, writing – review & editing.

Susanne Matschi: data curation, formal analysis, investigation, methodology, writing – review & editing.

Wolfgang Hoehenwarter: formal analysis, investigation, methodology, writing – review & editing.

Susanne Sachs: conceptualization, funding acquisition, investigation, methodology, project administration, resources, supervision, writing – review & editing.

9. Declaration of interests

The authors declare that they have no known competing financial interests or personal relationships that could have appeared to influence the work reported in this paper.

10. Data Availability

The proteomics dataset that supports the findings of this study is openly available on the ProteomeXchange Consortium via the Proteomics Identification Database (PRIDE) partner repository with the dataset identifier PXD028677 and 10.6019/PXD028677. A complete list of identified proteins can be found in Appendix B.

11. Figure legends

Fig **1**: Cell viability (a) and dry biomass (b) of a 96-h old tobacco BY-2 culture in MS medium sub-cultivated into MS_{red} and grown for 24 h. Error bars represent standard errors of the mean for one biological replicate with three counting events for MS medium and three biological replicates each with three counting events for MS_{red} medium. Statistical significance is denoted by * ($p < 0.05$) and *** ($p < 0.001$) between corresponding 0-h and 24-h samples. Micrographs of BY-2 cells before (c) and after (d) 24 h in MS_{red} medium. Scale bar: 20 µm.

Fig **2**: Internalisation of the FM4-64™ stain after 90 min of dye exposure in untreated tobacco BY-2 cells (Ctrl), cells treated with 20 µM uranyl(VI) nitrate and cells treated with both 20 µM uranyl(VI) nitrate and 5 µM wortmannin (WM). Cell physiology is shown by phase contrast images (a, c and e), and endocytosis is shown by FM4-64™ fluorescence (b, d and f). Scale bar: 50 µm.

Fig 3: Signal intensities from within the cell after 90 min of FM4-64™ in untreated tobacco BY 2 cells (Ctrl; n=61), cells treated with 20 µM uranyl(VI) nitrate (U; n=43) and cells treated with both 20 µM uranyl(VI) nitrate and 5 µM wortmannin (U+WM; n=42). Measurements are taken from at least two sampling events from one biological replicate for each testing condition. Statistical significance is denoted by *** ($p < 0.001$) between U and U+WM and n represents the number of cells per field of view.

Fig **4**: Uranium bioassociation to untreated BY-2 cells (control), cells treated with 20 µM uranyl(VI) nitrate (+U) and cells treated with both 20 µM uranyl(VI) nitrate and 33 µM wortmannin (+U +WM) for 6 h. Error bars represent standard errors of the mean. *** represents statistical significance between +U and +U+WM where $p < 0.001$.

Fig **5**: Bright-field transmission electron micrograph (a) of uranium-containing needle-like structures in tobacco BY-2 cells exposed to 20 µM uranyl(VI) nitrate for 24 h. EDX-based elemental mapping (b, c and d) is shown for the structures in a, with c and d containing overlays

of various signals. CW: cell wall; N: nitrogen; O: oxygen; P: phosphorus; S: sulphur; U: uranium; scale bar in element distributions: 100 nm.

Fig **6**: Uranium adsorption and precipitation in tobacco BY-2 cells exposed to 200 µM uranyl(VI) nitrate for 24 h. EDX sum spectra in panel d are from selected regions in the electron micrographs in a, b and c, labelled A1, B1 and C1, respectively, and the sum spectra from f are from selected regions in panel e, labelled E1-E4, to show the presence of uranium. CW: cell wall; M: mitochondria; PM: plasma membrane; V: vacuole; scale bars: 500 nm in a, 200 nm in b and e. The dotted lines in the spectra of d and f point to the position of the $L_{\alpha 1}$ peak of uranium (13.612 keV).